IV POLYMER IN FIBER FORMATION

Polymer properties have been discussed in the preceeding chapters. The description was given from the point of view of those properties which are accessible analytically, using more or less standard characterization techniques. The dynamics of the process require us to take another look at polymer properties, a look from a different angle. It is necessary to be able to understand how a polymer behaves within the complex maze of changes and transformations taking place either simultaneously or during a very short span of time. The specifics of the fiber formation process put more stringent demands on some polymer properties, which for other methods of processing may be less important or outright not essential. There is also a question whether the behavior of polymer in the fiber formation process can be predicted on the basis of analytically accessible characterization. Answers to such questions will be sought in the following considerations.

IV.1 Melting of polymer

The question to be posed initially regards the temperature at which the polymer ought to be processed. To answer this question, two aspects must be considered:

Primo — polymer viscosity must be within a range allowing processing: the polymer must be extruded through an appropriately sized capillary without the use of excessively high pressure to drive the extrusion.

Secundo — if the polymer is able to crystallize, or to form some kind of molecular aggregates, then the processing temperature must be higher than the equilibrium melting point (or an equivalent transition point). Otherwise, control of the development of crystallinity (or other structural units) in the fibers may become impossible.

Determination of the relationship between crystallization and melting temperatures, as described in chapter II, resolves this question, as does the determination of the relationship between melt viscosity, on one side, and shear rate and temperature, on the other side. If a polymer is heated to its equilibrium melting point, then all the crystals melt. However, the notoriously high viscosity of polymers does not allow for a very quick "randomization" of the molecular conformation. This "randomization" process may be helped by mechanical means, particularly by shearing forces. Additional elevation of temperature beyond equilibrium melting point by some twenty degrees centigrade may also be recommended. In the case that a polymer does not meet the above specified requirements for minimum of melting temperature, then methods of fiber formation other than from the melt, ought to be considered. Namely, one may escape to formation from solution. The upper limit of melting temperature depends on the thermal stability of the polymer under consideration. For the majority of industrial processes of fiber formation, the residence time of polymer at melt temperature ranges between some twenty and thirty minutes. Thus, polymer must be able to withstand the temperature for such a length of time. Again, if a polymer does not meet this requirement, fiber

formation from solution should be considered.

Polymer degradation rarely displays a strong transition point in the rate - temperature relationship. Therefore, the reader must be warned about many "grey areas" and difficult decisions as far as this aspect of processing is concerned.

At this point it is important to note that substantial differences in the behavior of polymers do exist. In practically all cases, exposure of the polymer to an elevated temperature ought to be in absence of oxygen (air). Almost all polymers are prone to some oxidation at elevated temperature. The oxygen molecules usually become randomly built-in along the molecule chains. An addition of atoms or groups changes the molecule symmetry, and thereby affects polymer crystallizability and crystallization kinetics. Often polymers are sensitive to moisture at elevated temperature; this concerns primarily polycondensation type polymers which may hydrolyze. Hydrolysis reduces the molecular mass, while in polycondensation reactions high molecular mass is difficult to obtain. Also, changes of molecular geometry may result from reactions with water molecules. Some polymers may show a tendency to increase their viscosity with increasing residence time at high temperature. Polymers obtained as a result of polycondensation reactions are more apt to such a behavior. A cross linking reaction is often responsible for the viscosity increase; increase of elastic flow component usually accompanies such an increase of viscosity.

Proper chemical stabilization of the polymer may prevent or reduce the changes, generally referred to as *degradation*, to some acceptable level. This is, however, a domain of polymer chemistry, and as such is outside of the scope of this book.

Practically all "virgin" polymers do contain some amount of cross linked material. The cross linked material is usually recognizable as gel inclusions, rather than an "impurity" homogeneously distributed throughout the polymer. The presence of cross links is often the result of side reactions typical of organic synthesis. The gel content in the polymer represents an important reason for breaks of polymer stream during fiber formation. Quantitatively, the process discontinuity is in direct proportion to the amount of cross linked material present in the polymer. It seems that both the increase of melt elasticity and the material inhomogeneity are responsible for the negative effects. The increased discontinuity of a process represents, naturally, a very strongly negative economic factor.

A somewhat "special problem" are the polyolefines. The nature of the stereospecific (Ziegler-Natta and similar) catalysts is such that it is more economic to obtain high, rather than low, molecular mass polymers. This fact led to the very common practice that polymers are polymerized to a high molecular mass (usually in the neighborhood of one million Daltons) and later degraded to smaller molecules. Since shear degradation in extrusion is expensive because of high energy consumption, the process is usually aided by the addition of peroxides.

The reactions between peroxides and polyolefines lead initially to formation of cross links. Only during the later stages do the cross link points decompose with the resulting chain scission. It may be easily established analytically that the reactions are usually incomplete: there are residual peroxides, as well as a number of

cross links. Such raw materials may pass for some low grade fibers. Processing of highly cross linked polymers may not be done under a positive control; melt elasticity increases very substantially, as may be seen from a comparison of calculated and experimental relaxation times.[70a]

Naturally, an increase of elasticity has its influence on the polymer processability. The cross links do not seem to be evenly distributed, but instead form gel aggregates which often may even be observed microscopically in polarized light. Analytically, the gel content is determined gravimetrically by pressure filtration of very diluted (0.25 to maximum 0.5 per cent) polymer solution through a filter of 0.24 to 0.5 μm pore diameter. Molecular mass and viscosity of the polymer at hand will determine the actual experimental conditions within the given ranges.

The molten polymer is usually transferred to a so called *spinning block* or *spinning beam* which, aside from the metering pump and spinnerette, also houses a filter for polymer melt. The filter is usually located as close to the spinnerette entry as possible and consists of a sintered metal plate supported on a perforated metal disc. The filters are to retain accidental mechanical contaminants, as well as insufficiently dispersed delustrants (usually titanium dioxide), pigments, stabilizers, etc.

Because the polymer must pass through the small and tortuous channels of the filter, it becomes subjected to large shearing forces. The shearing forces, if not excessive, are beneficial to fiber formation process. One of the characteristic properties of polymers is memory. The term memory means that different specimens originating from the same polymer may possess somewhat different properties, depending on the history of shearing and heat treatment to which they were subjected.[1,2] It is believed that the reason underlying the phenomenon of memory are frozen stresses.[3] However, a particularly strong influence are entanglements of the polymer chain. And, naturally, all these are highly dependent on relaxation time. It has been determined that entanglements of polymer chains determine physical and rheological properties of melts and solids.[3]

Recent years have brought an increase in research activity on polymer chain entanglements, and as a result, some quantitative solutions have become available.[4] One may quote as one of the more general formulations the finding by Elias[5] that the Hooke number,

$$He \equiv \frac{\sigma_b}{E\varepsilon_b} \tag{IV.1}$$

is proportional to the inverse square of the density of entanglements, μ_e. Here σ_b is tensile strength at break, ε_b is strain at break, and E is tensile modulus (initial). The entanglement density is:

$$\nu_e = \frac{N_A\,\rho}{M_e} = \left(\frac{9}{4}\right) \times \frac{N_A\,\rho}{M_c} \tag{IV.2}$$

where N_A is Avogadro's number, ρ is density of amorphous polymer, M_c is critical molar mass above which entanglements can form, and M_e is average molar mass between the points of entanglement. The value of M_e may be determined from the

plateau of the relationship between the shear modulus and molecular mass.[6] The values of entanglement density, along with the molecule conformation (characteristic ratio), may also be calculated from the chemical structure of a polymer.[7] The calculated values are in quite fair agreement with those determined experimentally, though the experimental results have relatively large uncertainty too.

It is also well known that flow can either cause transformations like crystallization, mixing, and demixing, which normally result from temperature change, or may shift the temperature at which the transformation takes place.[8]

Determination of the exact changes in the molecule conformation and entanglements due to polymer flow is very complex. Therefore, there is still disagreement between some of the results published. It is known, however, that besides the flow intensity, as described by strain or strain rate, entanglements depend strongly on the type of flow, and on the geometry of the duct.[8,9]

IV.2 The Spinnerette

The spinnerette (or spinning jet) is the element of fiber formation hardware which serves to shape the polymer melt, or solution, into "infinitely long" cylinders. Since the heart of the spinnerette is the capillary, everything that applies to flow in a capillary also applies to flow in spinnerettes. The side phenomena which result mainly from the shearing action on the extruded polymer, have a strong influence on certain engineering tasks and on the behavior of the polymer in the subsequent processing stages. Ultimately, the shearing applied influences the final fiber properties. Here we have a certain similarity between the influence of spinnerette and filter on the processing performance of the polymer and on the final result, on the fiber properties.

The shearing a polymer experiences in the spinnerette influences the morphology of polymer melt. Some light on these influences is shed by the work of Han and Kim.[8] Fig. IV.1 shows an essential result obtained by Han and Kim: the relationship between pressure exerted by the polymer on the wall of the reservoir and capillary *versus* distance from the entrance to the capillary. The plot shows clearly the pressure loss in the entry to the capillary and the normal pressure present in the polymer at the exit from the capillary.

The exit pressure for a given geometry of the extrusion arrangement and conditions is $P_{ex} = \alpha\dot{\gamma}^{\beta}$. In this case α and β are constants characteristic for the material. The true shear stress at the wall may be calculated from the slope of the straight portion of the axial pressure profile, e.g. like in figure IV.1.

$$\tau_w = \left(\frac{-\partial p}{\partial x}\right) \times \left(\frac{D}{4}\right) \tag{IV.3}$$

In view of the above, it is clear that evaluation of the capillary flow data with the use of the common equation (equation III.4) or in the version suggested by

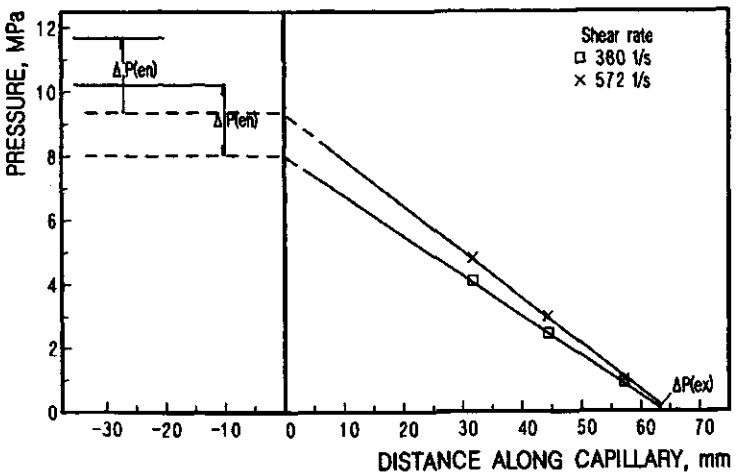

Figure IV.1: *Pressure profiles in reservoir and in capillary during extrusion of polyethylene at 180 C, capillary L/D = 20, the ratio of reservoir over capillary diameter is 9. After Han and Kim.*[8]

Bagley

$$\tau_w = \frac{\Delta P - \Delta P_{en}}{4\,(L\,/\,D)} = \frac{\Delta P}{4\,(L\,/\,D)\,+\,e} \tag{IV.4}$$

where ΔP is pressure difference necessary for extrusion, ΔP_{en} pressure drop in the entry to the capillary, D is diameter of the capillary, L is the length of the capillary, and e is the *"end correction"* according to Bagley.[10]

Han and Lamonte[11] have established that the pressure at the exit from the capillary equals the normal stress difference at this point:

$$P_{ex} = P_{11} - P_{22} \tag{IV.5}$$

From figure IV.1, one may see the magnitude of the pressure drop in the entry to the capillary for different shear rates. Figure IV.2 shows an influence of the ratio of reservoir over capillary diameters on the exit pressure. The repercussions of the flow pattern are far reaching indeed. Comparison of figure IV.2 with figures III.17 and III.18 is quite instructive.

Apparently the geometry has a strong influence on the vortices formed around the entry. The influence becomes insignificant above some value of reservoir to capillary ratio; for polyethylene investigated, this significant ratio is above 12, for other polymers may be somewhat different. The influence of conical entry to capillary, and of the magnitude of the cone angle on the process of extrusion was investigated, to some extent, by Han.[9] Direct measurements of pressure in the capillary, entry cone, and reservoir were conducted, similarly as in the earlier work by Han. It has been found that the magnitude of the pressure loss in the conical entry to the capillary depends on the cone angle. The minimum value seems to be reached in the entry of ninety degrees. However, the large scatter of the experimental data makes this minimum uncertain. The differences in the

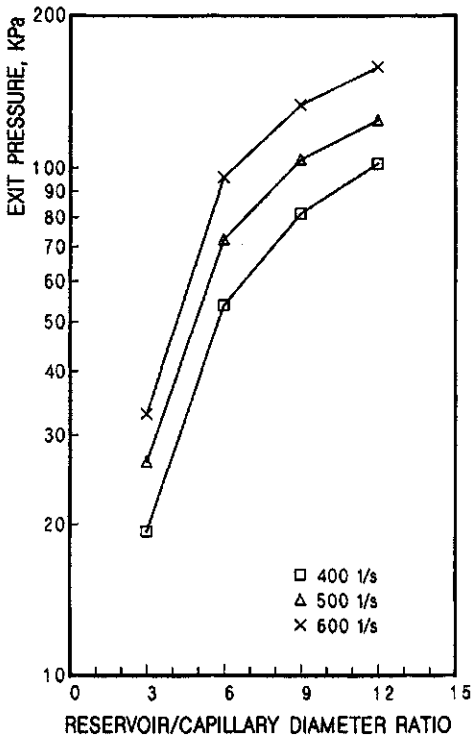

Figure IV.2: *Relationship between exit pressure drop and ratio of reservoir to capillary diameter ratio. After Han and Kim.*[8]

pressure loss for angles ranging from sixty to one hundred eighty degrees are small indeed. On the other hand, for angles of thirty degrees the pressure rises some twenty to thirty per cent, and for those of fifteen degrees, the pressure drop almost doubles.

The angle of the entry cone has significant influence on the exit pressure. In this case, the results for angles between sixty and one hundred and eighty degrees are similar, within large data scattering. For small angles, fifteen to thirty degrees, the exit pressure reaches values as low as one half of the results for large entrance angles. These results are in full agreement with those published elsewhere.[12] The data by Han[9] tend to indicate that the exit pressure for low cone angles and for high cone angles would be the same at shear rates of around 1500 s^{-1}. Other investigations[1,13] do not confirm such behavior, though carried out at shear rates as high as 7500 s^{-1}.

The results obtained by Han[9] show a difference in the behavior of high density and low density polyethylenes. Perhaps a different level of elastic flow component is responsible for this.

It must be added that the Poiseuille equations for flow in capillaries (equations III.3 to III.5) are valid for Newtonian fluids, characteristic of strictly parabolic velocity profile, or in other words for power law fluids with the exponent equal

unity. A generalization based on the power law leads to the velocity distribution along the capillary radius as[17]

$$V(r) = V(0)\left[1 - \left(\frac{r}{R}\right)^{(n+1)/n}\right] \tag{IV.6}$$

where $V(r)$ is velocity at radius r, r is position along the radius, R is capillary radius, and n represents the power law coefficient. Furthermore, the relationship between the polymer flow and the extrusion driving pressure may be presented in a general form as

$$Q = \left[\frac{n}{(n+1)}\right]\pi R\left[\frac{(\Delta P\ R^3}{(2\eta l)}\right]^{1/n} \tag{IV.7}$$

The velocity gradient then becomes

$$\dot{\gamma}\left(\frac{\partial V}{\partial r}\right)_{r=R} = -\left[\frac{(\Delta P\ R)}{(2\eta l)}\right]^{1/n} \tag{IV.8}$$

In the above equations l stands for the capillary length.

All of the equations for capillary flow as given above are valid for infinitely long capillaries. In the capillaries of finite length, and such we have in spinnerettes, the effective pressure, ΔP_e, is different from the pressure really applied, ΔP, and the difference may be given as

$$\Delta P_e = \frac{\Delta P - m\rho V_0^2}{1 + (r\ /l\ ))\,(k + (S_R\ /\ 2) + z\,(t\ /\tau)} \tag{IV.9}$$

where $V_0 = Q/\pi R^2$ is the average flow velocity, m is a coefficient dependant on the velocity profile, for Newtonian fluids $m = 1$, for polymer melts it may be taken as $m = 1.2$, ρ is polymer density, S_R is recoverable strain, t is transit time.

Viscoelastic fluids require also a longer time to develop stable flow. This translates naturally to an extended capillary length. Zahorski[28] has derived a correction for the capillary length in the form

$$\Delta l = \frac{l_v[(\Delta P_e - \Delta P) + (p_{11} - p_{22})]}{\Delta P_v} \tag{IV.10}$$

where Δl is the additional capillary length needed, l_v is the length of capillary needed to achieve stable flow of Newtonian (viscous) fluid, ΔP_v is the driving pressure for extrusion of viscous fluid, $p_{11} - p_{22}$ is normal stress difference. There is, however, a problem with the determination of the l_v value; the equation derived for the purpose by Goldstein[27] is inapplicable for viscoelastic fluids.

Thus, it may be seen that calculation of the capillaries for viscoelastic fluids may not be so simple, or so accurate. It may be necessary to apply special solutions involving constitutive equations for the specific case on hand.

A relatively large effort has been devoted to determining the influence of various modes of flow, as well as of the flow intensity, on the resulting polymer morphology, and ultimately on the corresponding polymer properties.[2,12–15] The results

obtained thus far and the conclusions offered by various authors are not entirely coherent. There are only few points to be stressed with some certainty. Namely:

- The effect a flow has on the polymer depends on the polymer type, *e. g.* noncrystallizable, block copolymer (thermoplastic elastomers), thermotropic liquid crystalline.[15]
- The effect of flow depends on its mode and geometry, *e. g.* shear, elongational, curvilinear.[8,15]
- Orientation caused by shear relaxes faster than it might be measured by any reliable technique.[13,15]
- In extensional flow, the polymers with flexible chains seem to be oriented to a degree too small to be measurable by any proper, currently available techniques.[13,15]
- Liquid crystalline polymers do not become oriented in a shear flow, while they become strongly oriented in extensional flow.[15,138]
- In melt shearing of A-B-A copolymers, the hard segments become little elongated.[15]
- Changes in entanglement density due to perturbations in flow, (*e. g.* tumbling of coiled molecules in shear flow) do not necessarily lead to orientation effects, but they certainly do lead to an increase in strength.[13]

Experience tells us that the quality of fibers and the ease of processing increase with increasing length of spinnerette capillary. But it also increases with increasing shear rate in the capillary.[13] The effect is most likely related to the increasing number of entanglements due to shear rate. The increased relaxation in long capillaries probably reduces the stresses to which the entangled chain segments are subjected, but without reducing the number of entangled chains. In effect, the die swell decreases, so the required attenuation of the fiber diameter is smaller. However, the mechanical strength of the fibers increases markedly with increasing shear rate in the capillary. Shear rates as high as $7500s^{-1}$ have been used with a substantial success. Nevertheless, in application of the high shear rates and large capillary length, one meets an overpowering challenge: the requirement of high extrusion pressures. Thus, technologically reasonable solutions will dictate where the right compromise lies. Besides, the critical shear rate, which is a complex result of polymer nature, geometry of equipment, and extrusion conditions, imposes another limitation on the intensification of the process. The phenomenon of extrudate fracture has been discussed in section III.8.

IV.3 Forces Acting in Quench Zone

An analysis of the forces acting on the filaments in the quench zone was conducted by Ziabicki and co-workers in the early sixties and later summarized in his

books.[16,17] The force balance has been determined to be

$$F_e + F_g = F_r + F_i + F_s + F_a \tag{IV.11}$$

where F stands for force, and the subscripts are: e – external (drawing), g – gravity, r – rheology, i – inertia, s – surface, and a – aerodynamic.

The external force is, naturally, the force applied by the take-up rollers or aerodynamic jet. The question is: how large a force needs to be applied for a given process? This is the answer expected from the examination of the entire force balance.

The gravity force may be presented as

$$F_g = g\frac{(1-\rho_0)}{\rho} \times \cos\chi \tag{IV.12}$$

In equation IV.12 the notation is: g – acceleration due to gravity, ρ_0 – density of the surrounding, ρ – density of filament, χ – angle between the filament and the horizontal. For the vertical formation, χ is 90°, provided that the path of the spinline is not altered, *e. g.* by a cross flow quench air. For horizontal spinning, wet processes included, χ equals 0. However, the line is normally deformed either by gravity or by buoyancy. The deformed line usually assumes a form of hyperbolic cosine (chain curve). Much more serious inaccuracy of equation IV.12 is connected with the change of filament density from that of a melt (or solution) all the way to a semicrystalline solid. As the changes of density are difficult to express in a form of a function, exact solutions need to involve numeric integration to take care both of the density changes and of the potential changes of the angle χ.

In case of vertical formation path, the gravity force acts in the same direction as drawing force. In horizontal configuration, some components of the gravity force may act in the same direction as gravity force, though on some sections of the spin line the force components may act in the opposite direction. All of the remaining forces act in the direction opposite to the drawing force.

The force needed for acceleration of the material (the force of inertia) has been described as

$$F_i(x) = \rho\, Q\, (\psi\, V - \psi_0\, V_0) \simeq \rho\, Q(V - \psi_0\, V_0) \tag{IV.13}$$

where x is distance from the spinnerette, ρ stands for polymer density at point x, while ρ_0 is initial polymer density, V is filament velocity at point x, and V_0 is initial polymer velocity, ψ represents a coefficient describing the velocity profile, the subscript 0 indicates a parabolic profile, for a flat velocity profile ψ equals unity. Since the overwhelming majority of the spinning path has a flat, or nearly flat, profile it is justified to simplify the equation to IV.13.[2] However, similarly as in the case of gravity, the changes of filament density are difficult to depict in the form of a function. Therefore, analytical solutions of equation IV.13 must be considered as quite inaccurate. The force of inertia is, naturally, acting in the direction opposite to the drawing force.

The surface force results from the interfacial tension between the filament surface and the surrounding medium, and from the change of filament curvature.

$$F_s = \pi \nu [R_0 - R \vartheta(x)] \tag{IV.14}$$

Here ν represents interfacial tension, R is fiber radius, while other notation is as above. Due to changes of temperature of the melt, surface tension may change by some ten per cent. For accurate results, temperature correction should be in place. In case of fiber formation from solution, changes of temperature may be not quite as large, but changes of polymer - solvent composition may have a much larger effect on surface tension and the appropriate corrections should by no means be neglected.

The forces of material deformation (the rheology force) have been treated by Ziabicki[16,17] in a very schematic and sketchy fashion. As may be seen from figure IV.3, the deformation forces are quite dominant in the process and must be considered much more seriously.

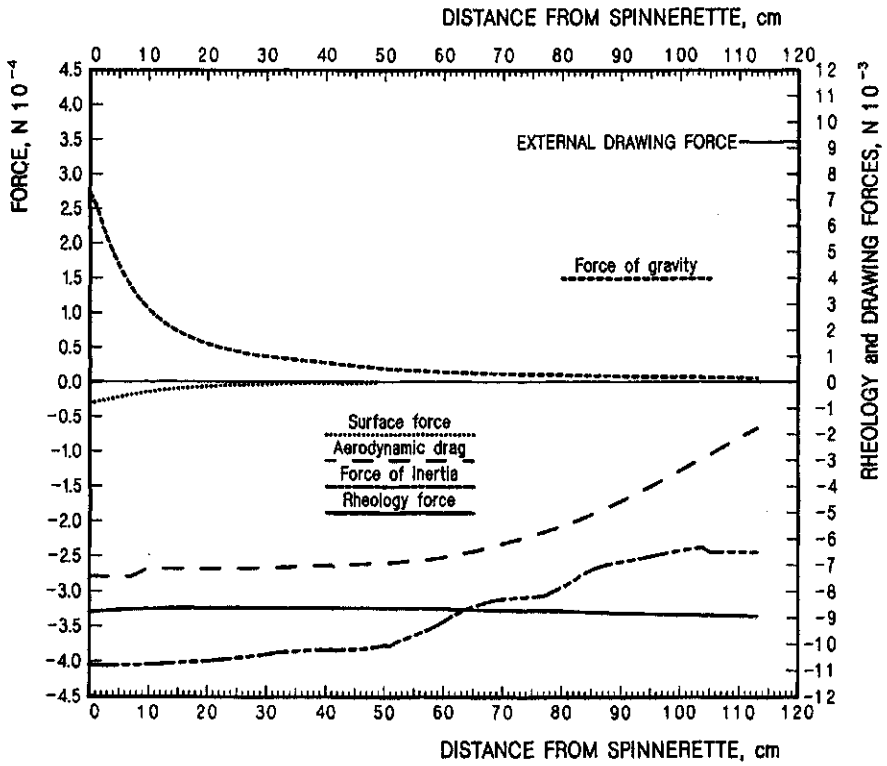

Figure IV.3: *Forces acting on a filament in quench zone. Medium fast process. Details in text. Note the different scales on the force axis.*

The next section on melt drawing reviews the status of that knowledge as of now.

The same may be said about the aerodynamic forces. The matter is considerably more complex than originally depicted by Ziabicki.[16,17] The magnitude of the forces present in industrial fiber formation, particularly at moderate and high velocities, brings them to a level comparable to the rheology forces. The flow of a large volume of air through the fiber paths, sometimes consisting of substantially more than a thousand filaments, makes things much more complex. These problems are discussed in the chapter on engineering physics. Figure IV.3 presents forces acting on a filament in an industrial process of fiber formation with final velocity in excess of 4000 m/min. The last point on the graph corresponds to 955 m/min. The polymer used was polypropylene of weight average molecular mass of 230 000. The data were collected during a detailed process analysis. Total external drawing force applied was 0.025 N per filament. The data for rheology forces result from the force balance, while all the other data result from calculations based on measured process parameters. For better visualization of the relative magnitude of the various forces, as well as for visualization of the shape of the curves, different scales have been put on the force axis.

IV.4 Diameter Attenuation

Upon leaving the spinnerette, the polymer stream is usually extended, which leads to a decrease of the filament diameter. It would be exceedingly difficult to extrude fibers of the final diameter, or the diameters would have to be very, very coarse indeed. The extension, as will be discussed below, has several more reasons and/or consequences than just diameter attenuation. The extension process brings, naturally, a question: will the filament break or not? Molten polymer, or polymer solution, intuitively are not expected to be able to withstand any significant stresses.

Nitschmann and Schrade[18] attempted to explain the extension- attenuation process in fiber formation by taking advantage of the Trouton studies[19] on extension of amorphous liquids. The work of Nitschmann and Schrade led to the construction of an interesting instrument, a kind of balance, for determination of extensional viscosity of polymer solutions. Determinations of extensional viscosity of casein fiber dope* and of solution of nitrocellulose, using Nitschmann and Schrade's "balance", gave interesting insight into the problems. It was found that elongational viscosity in its dependence on deformation rate, or on the stresses involved, shows quite different behavior than shear viscosity. This pioneering work, however interesting and important, brought more new questions than answers.

The important findings were that the extensional (Trouton) viscosity depends on the extension rate, similarly to shear viscosity. The similarity includes the fact that the relationship is not necessarily linear. In the nonlinear region, the shear and extension behavior are not necessarily parallel, or even similar. In both cases, though, when certain limiting value of deformation rate is exceeded, one observes

*solution for fiber formation

flow instability. It has been noticed also that as the filament diameter decreases (the extension increases), the filament is able to withstand higher force, extensional viscosity increases. The most striking observation was this: extensional viscosity showed a minimum in its dependence on stress (for casein fiber dope ranging from some 27 to 33 KPa, depending on the load, it is on rate of extension).

The first man-made fibers were obtained from polymer solutions; rupture of the filaments often led to break-up of the polymer stream into droplets. There were several attempts to devise a notion of *spinnability*[20–22], mostly involving viscosity and surface tension. In practice, however, the tests of spinnability were difficult to reproduce, impractical,[23] and therefore will not be elaborated on here.

The literature in the subject of elongational rheology and its application to fiber formation is sizeable. In 1979, C. J. S. Petrie[24] devoted to the subject a quite extensive and detailed monograph. Many of the suggestions appear under names that are notable in the field of rheology. Yet, the problems of elongational flow in fiber formation is deemed far from being solved. V. Tirtaatmadja and T. Sridhar[150] have tested experimentally application of various constitutive equations to extensional flow. Out of the models, Oldroyd - B, Gieskus, Perne, and White - Metzner with application of multiple retardation times, the best result obtained was extensional viscosity within the correct order of magnitude. This is by far not enough. To cope with the large number of proposals which often represent very interesting exercises in theory of rheology, we shall look at the phenomenological picture of fiber formation, and on this basis we shall present those solutions which seem to be in the best agreement with the science of rheology, as well as with the process realities. We shall try to propose those solutions which appear to carry the better promise. Figure IV.4 represents the events covered by the term "melt drawing". Section A of the figure gives a schematic pictorial representation, while section B presents a concretization of the scheme in the form of the pertinent analytical data collected in an commercial process of rather fast fiber formation (4070 m/min final fiber velocity) from polypropylene.

One may assume that after passing through filters, the polymer is "stripped of its memory". In reality, the history goes back to the moment of polymerization, but the intensive shearing may be able to reduce, or overpower, the remnants of the previous history to a negligible level. If so, than the meaningful history starts with the moment the polymer enters the spinnerette, the counter bores leading to the capillaries. As the introducing channels usually have a conical section leading to the capillary proper, the polymer is subjected to shearing and to extensional[25,26] deformation, which are superimposed on each other (see also sections III.6 and III.7). The elongational deformation imposed in the conical entry to the capillary relaxes to some extent in the cylindrical section of the capillary. Nevertheless, upon exit from the capillary the remaining elongation relaxes further, and together with the change of the parabolic velocity profile to a flat one, this causes the polymer stream to swell. There is a strain, or force, applied on the other end of the polymer stream.

In the example given in Figure IV.4 B, at the exit of the spinnerette, the stress

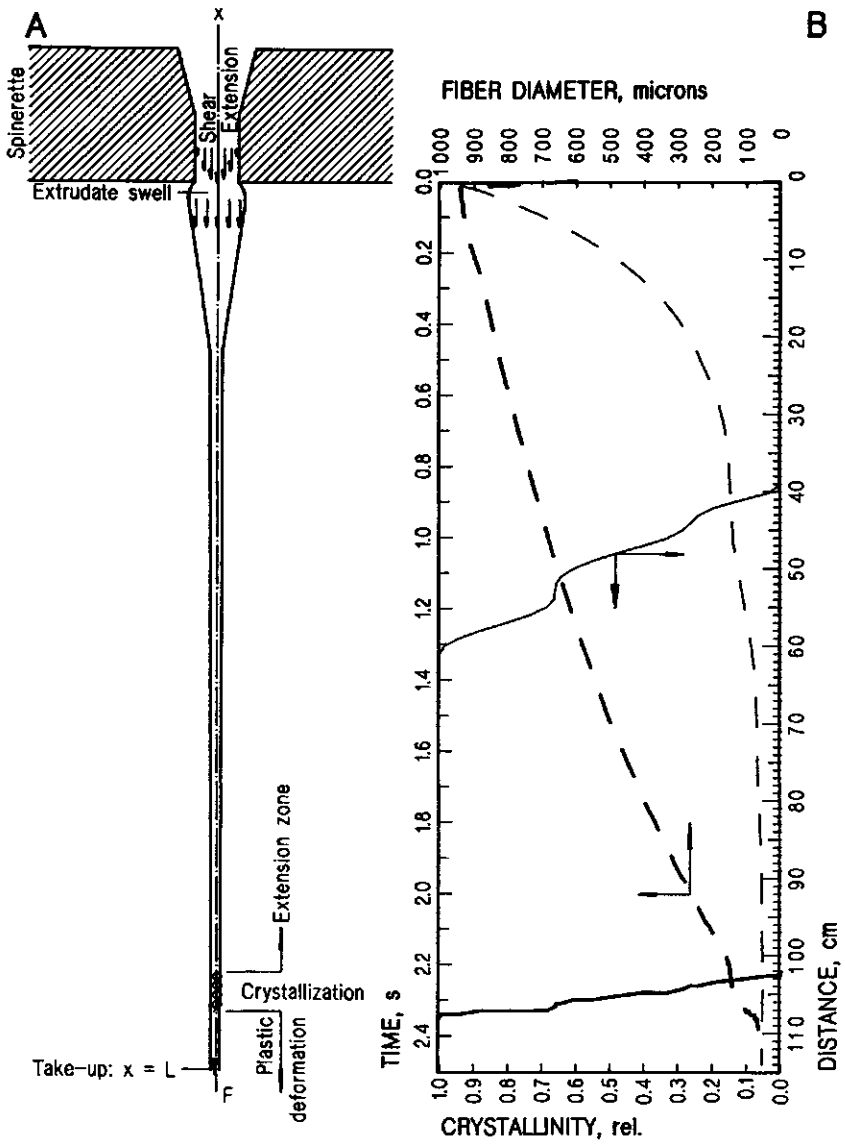

Figure IV.4: *A: Schematic representation of polymer flow in fiber formation. B: Diameter change (dashed lines) and crystallization (full drawn lines) against distance (fine lines) from spinnerette and against time (heavy lines). Analytical data from a commercial process.*

exerted by the drawing represents 14.5 per cent of the pressure needed to push the polymer through the cylindrical section of the capillary. It is true that the process

is quite fast, for slower processes the stress may fall down to 5, or even 3 per cent. However, for some processes, especially those faster ones, it may reach even 20 per cent. The range of stress cannot be considered negligible, and it should be taken into account in the capillary flow calculations as a negative pressure. The drawing stress, whatever its level, is insufficient to prevent the extrudate swelling completely, though it may diminish it. From the point of the maximum swell, begins the diameter attenuation. The attenuation process normally continues until final take-up of the ready fibers.

IV.4.a Basic Mechanics of Drawing

The initial portion of attenuation, by definition, proceeds according to the laws of elongation, extension, or stretching, depending on the preferred nomenclature. The initial segment of the process, where melt rheology ought to rule, ends when the polymer starts to crystallize. The initial stages of crystallization may also be possibly treated according to the melt rheology rules, but the material properties change quite dramatically and fast. Larger crystallization nuclei and small crystallites in the process of growing may act as points of cross linking. In the latter case the material would change from rheodictic into arrheodictic, and it would be subject to somewhat different rules of rheology; studies of these problems are in their infancy.[131]

When the crystallization process is completed, or nearly so, the material may be deformed according to the principles of plastic deformation. If one examines the course of crystallization in figure IV.4 B, then it is easy to find two "yield" segments, which may be read as a kind of change in the mechanism of diameter attenuation due to change of the material properties.

It is necessary to stress that the described process is accompanied by cooling, and in the depicted case, the cooling was rather intensive. And that is the way it is with almost all fiber formation processes, down to the start of crystallization, or other phase transition. The only exception may represent some wet process. However, the process of crystallization, as all other processes of phase transformation are, is exothermic. Exothermic is also plastic deformation. Thus, from the onset of crystallization, the processes are never isothermal.

It is necessary to point to the difference of interpretation of the process in terms of distance from spinnerette face and in terms of time. The curves plotted against time are usually smoother. The most striking may be a comparison between the crystallization process taking 35 cm distance (from 28 to 63 cm) but taking only 120 ms.

Among the more important efforts on a theoretical solution to the problem of material strength in extension, one must certainly quote that by M. Reiner and A. Freudenthal.[29] These authors extended the material strength theory on the basis of the maximum of distortional energy by M. T. Huber and H. Hencky. The static concept of distortional energy, E_0, has been substituted with the dynamic concept of the *power of distortion*, dE_0/dt. Further, the authors recall the representation

of the different forms of mechanical energy, as proposed by K. Weissenberg (figure IV.5). From the figure, it is evident that the sum of energies at any point of the triangular area, $E_K + E_P + E_D$, must equal the work of the external forces. The distortional energy is then, $E_0 = E_P + E_D$.

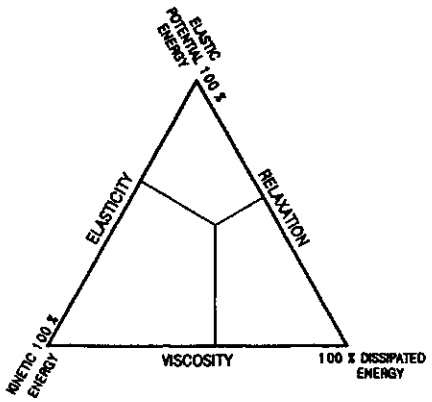

Figure IV.5: *Representation of the body conditions upon an input of energy, according to K. Weissenberg as cited in ref. 29.*

As the first condition, the Huber-Hencky theory states that *failure by distortion is governed by the maximum value of the elastic energy of distortion.* The modified formulation by Reiner and Freudenthal is given the following form

$$\int_{t=0}^{T} \frac{dE_P}{dt}\, dt = \int_{t=0}^{T} \frac{dE_0}{dt}\, dt - \int_{t=0}^{T} \frac{dE_D}{dt}\, dt \qquad \text{(IV.15)}$$

The kinetic energy influences the strength only in case of impact. In such cases, the kinetic energy becomes transformed into hydrostatic tension, which may lead to a failure. The second condition of the Huber-Hencky theory concerns cases when the rate at which the energy is transformed exceeds the ability of the material to be strained, *e. g.* if the magnitude of tensile stress caused exceeds the actual cohesion of the material.

Equation IV.15 implies that certain amount of the distortional energy may be dissipated during the time of the event. The dissipation is due to a viscous or/and plastic flow. In case the rate at which the distortional energy is delivered equals the rate at which the energy is dissipated,

$$\left(\frac{dE_0}{dt}\right) - \left(\frac{dE_D}{dt}\right) = 0 \qquad \text{(IV.16)}$$

then there is practically no limit to the amount of the distortional energy which might be supplied to the material without causing a failure. This is a case of *creep.*

By taking advantage of the Maxwell body, the authors[29] arrive at the following basic equations:

$$\left(\frac{1}{A}\right)\frac{dA}{dt} = -\left(\frac{1}{3\,E}\right)\frac{d}{dt}\left(\frac{P}{A}\right) - \left(\frac{1}{3\,\eta}\right) \times \left(\frac{P}{A}\right) \tag{IV.17}$$

The distortional energy is given as

$$E_0 = \frac{1}{6\,E}\int_{t=0}^{T} \frac{d}{dt}\left(\frac{P}{A}\right)^2 dt + \frac{1}{3\,\eta}\int_{t=0}^{T}\left(\frac{P}{A}\right)^2 dt =$$

$$= \frac{1}{6\,E}\left[\left(\frac{P}{A}\right)^2 - \left(\frac{P_0}{A_0}\right)^2\right] + \frac{1}{3\,\eta}\int_{t=0}^{T}\left(\frac{P}{A}\right)^2 dt \tag{IV.18}$$

In the above equations we have: P - force, A - area of cross section, E - modulus, η - viscosity, l - length, subscript 0 denotes initial value. Stress, $\sigma = P/A$, as a function of time needs to be determined by taking advantage of equation IV.17. Reiner and Freudenthal derive equations for several cases of deformation; for us, two of them may be interesting: constant velocity of strain and constant force.

For a case of constant velocity of strain the general equation has the form:

$$\frac{P}{A} = \exp(-t\ /\ \theta)\left[3\,E\frac{v_0}{l_0}\int \frac{\exp(t/\theta)}{1+(v_0\ t/l_0)}\ dt + \frac{P_0}{A_0}\right] \tag{IV.19}$$

The integral given in equation IV.19 has no finite solutions and cannot be solved by convergent series. The following approximate solution is suggested for cases with $0 \le \Delta l \le l_0$

$$\int \frac{\exp(t/\theta)}{1+v_0 t/l_0}dt = \int \frac{\exp(t/\theta)}{1+c_0 t/\theta}dt \simeq \exp\left[\frac{1}{1+2\ (c_0)^{3/2}} \times \frac{1}{\theta}\right] \tag{IV.20}$$

Here $c_0 = v_0\ \theta/l_0$ and represents the elongation at $t = \theta$. In this case velocity is constant: $v(t) = v_0 = const.$ The time-strain function is

$$\frac{\Delta l}{l_0} = \frac{c_0\ t}{\theta} \tag{IV.21}$$

The strain-stress function is given as

$$\frac{P}{A} = 3\ E\ c_0(1+2c_0^{3/2})\left[\exp\left(-\frac{2\ c_0^{3/2}}{1+2\ c_0^{3/2}} \times \frac{\varepsilon}{c_0}\right) - \exp\left(-\frac{\varepsilon}{c_0}\right)\right] \tag{IV.22}$$

where $\varepsilon = v\ t/l_0 \approx \Delta l/l_0$. The strain-load function has the form

$$P = \frac{3\ E\ A_0\ c_0(1+2c_0^{3/2})}{1+\varepsilon}\left[\exp\left(-\frac{2\ c_0^{3/2}}{1+2\ c_0^{3/2}} \times \frac{\varepsilon}{c_0}\right) - \exp\left(-\frac{\varepsilon}{c_0}\right)\right] \tag{IV.23}$$

The time-energy function is

$$E_0 = \frac{3\,E\,c_0^2(1+2c_0^{3/2})^2}{2}\left[\exp\left(-\frac{2\,c_0^{3/2}}{1+2\,c_0^{3/2}}\times\frac{t}{\theta}\right)-\exp\left(-\frac{t}{\theta}\right)\right]^2 +$$

$$+\,3\,E\,c_0^2(1+2c_0^{3/2})^2\left\{-\frac{1+2\,c_0^{3/2}}{4\,c_0^{3/2}}\left[1-\exp\left(-\frac{4\,c_0^{3/2}}{1+2\,c_0^{3/2}}\times\frac{t}{\theta}\right)\right]-\right.$$

$$-\,2\times\frac{1+2\,c_0^{3/2}}{1+4\,c_0^{3/2}}\left[1-\exp\left(-\frac{1+4\,c_0^{3/2}}{1+2\,c_0^{3/2}}\times\frac{t}{\theta}\right)\right]+$$

$$\left.+\,\frac{1}{2}\left[1-\exp\left(-\frac{2\,t}{\theta}\right)\right]\right\} \qquad \text{(IV.24)}$$

According to the above derivations, rupture occurs if

$$v_0\,[1-\exp(-t/\theta)] = \frac{[l_0\,(6\,E\,E_0)^{0.5}]}{(3\,\eta)} \qquad (IV.24\,a)$$

$$\frac{t}{\theta} = \ln\left[1-\frac{l_0\,(6\,E\,E_0)^{0.5}}{(3\,\eta\,v_0)}\right] \qquad (IV.24\,b)$$

As a consequence, if

$$v_0 < \frac{[l_0\,(6\,E\,E\,0)^{0.5}]}{(3\,\theta)} \qquad \text{then} \qquad \varepsilon_0 < \left[\frac{(2\,E_0)}{(3\,\eta)}\right]^{0.5} \qquad \text{(IV.25)}$$

All this means that the material can be strained indefinitely, so to say. Deformation under constant load, when $P = P_0 = const$, represents another possibility of interest in connection with fiber properties (creep), and in connection with diameter attenuation.

On integration of equation IV.17 one obtains

$$\frac{A}{A_0} = -\varepsilon_0 \ln\left(\frac{A}{A_0}\right) = 1-\frac{\varepsilon_0\,t}{\theta} \qquad \text{(IV.26)}$$

where $\varepsilon_0 = P_0/(3EA_0)$. Equation IV.26 may be simplified for commonly encountered cases when $A_0 \geq A \geq 0.5A_0$ as follows:

$$A = A_0\left(1-\frac{\varepsilon_0\,t}{\theta}\right) \qquad \text{(IV.27)}$$

When using this simplification one can obtain some important relationships. And so the time-velocity function is

$$v(t) = \frac{P_0\,l_0}{A_0\,3\,\eta}\times\frac{1}{[1-(\varepsilon_0\,t)/\theta]^2} \qquad \text{(IV.28)}$$

Strain as function of time

$$\frac{\Delta l}{l_0} = \left[\frac{\varepsilon_0}{1-(\varepsilon_0\ t)/\theta)}\right]\left(\frac{t}{\theta}\right) \tag{IV.29}$$

Stress-strain relationship

$$\frac{\Delta l}{l_0} = \frac{\sigma}{\sigma_0} - 1 \tag{IV.30}$$

where $\sigma = P/A$ and $\sigma_0 = P_0/A_0$ and by assumption $P = P_0 = const.$

Energy as function of time is described by

$$E_0 = \frac{1}{6\ E}\left(\frac{P_0}{A_0}\right)^2 \frac{1}{[1-(\varepsilon_0\ t/\theta)]^2} + \frac{1}{3\ E}\left(\frac{P_0}{A_0}\right)^2 \frac{1}{1-(\varepsilon_0\ t/\theta)} \times \frac{t}{\theta} \tag{IV.31}$$

Failure takes place if

$$\sigma_0 = [1-(\varepsilon_0\ t/\theta)](6\ E\ E_0)^{0.5} \tag{IV.32}$$

at

$$\frac{t}{\theta} = \frac{3\ E\ A_0}{P_0} - \left(\frac{3\ E}{2\ E_0}\right)^{0.5} \tag{IV.33}$$

The main reservation to the above proposals of solution to the problem is the use of the shear viscosity and shear modulus. It is known that the extensional flow cannot be described on the basis of experiments in shear.[24,30,31]

IV.4.b Extensional Flow Problems

Development of extensional rheometry remains far behind shear analytical methods. Reliable instruments have been developed only relatively recently. Understanding of the basic nature, and consequently, interpretation of the experimental results still seem to be rather unsettled, at best.

A very substantial effort in the investigation of extensional flow has been invested by G. V. Vinogradov and the team of his co-workers. Significant and exciting results were presented in 1970.[32,33]

Vinogradov's team built its own rheometer and investigated high molecular mass noncrystallizable polymers to make the experimental work simpler, and to avoid complications due to crystallization. A very important element of these investigations was determination of relaxation for every point of extension collected. The completeness of the data collected allowed evaluation exceeding the customary procedures, and in some ways was nonconventional.

The extensional deformation has been formulated according to the method of Hencky, $\varepsilon = \ln(l/l_0)$. Here ε is total deformation, l_0 is initial length of the sample, l is length of the sample at some time t; ε_e is elastic (reversible) deformation, while ε_i is irreversible deformation, $\varepsilon_i = \ln(l_i/l_0)$, where l_i is length of the fully relaxed

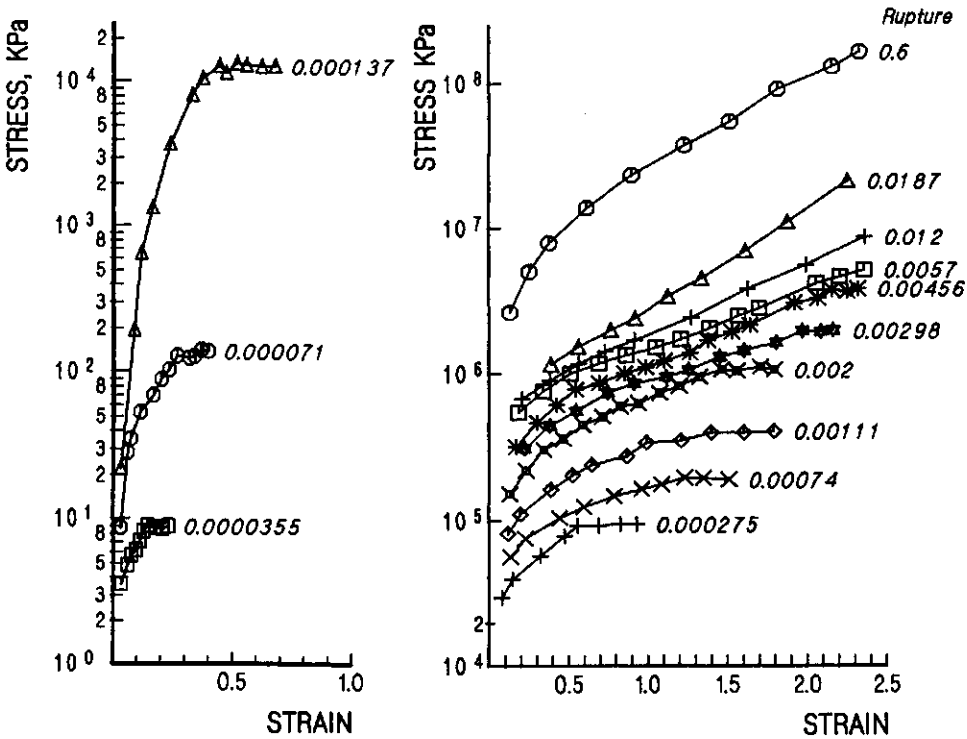

Figure IV.6: *True stress versus total strain for various strain rates (given as parameter). After G. V. Vinogradov et al.*[33].

sample, $\varepsilon_e = \varepsilon - \varepsilon_i$. Extensional viscosity is $\zeta = \sigma/\dot{\varepsilon}_i$, where σ represents true stress and $\dot{\varepsilon}_i$ stands for the rate of irreversible deformation. Modulus of elasticity is $E = \sigma/\varepsilon_e$.

From figure IV.6 - left, one may see that for low deformation rates, the true stress rises monotonically with strain to reach a plateau representing a constant value of stress at $\varepsilon = \dot{\varepsilon}_i = const$. With the increasing extension rate, the shape of the curves gradually change from convex toward stress axis, further to assume an S-shape, and further, at still higher extension rates, the plateau region disappears, up to the point of rupture. For those conditions where the constant stress is observable, the time, t_s, and deformation ε_s, where the constant stress begins, change rapidly with strain rates. This may be seen in figure IV.7. The onset of constant stress flow coincides with the maximum in the elastic deformation.

Figure IV.8 presents extensional viscosity on total (top) and on irreversible deformation, deformation rate is given as a parameter. One may notice that for some deformation rates, viscosity reaches a constant value independent of deformation. Before the region of constant value is reached, viscosity may pass through a maximum. Such a maximum is located in the vicinity of the point where the reversible and irreversible deformations are equal. Initially, viscosity grows with

increasing strain nearly linearly, especially if the irreversible strain is considered. The same is true independently of the rate of strain. The length of the nearly linear segment of the curve extends toward higher deformation as deformation rate increases. Eventually, a level of deformation rate is reached where the entire curve is linear, without a maximum, without a segment of constant viscosity.

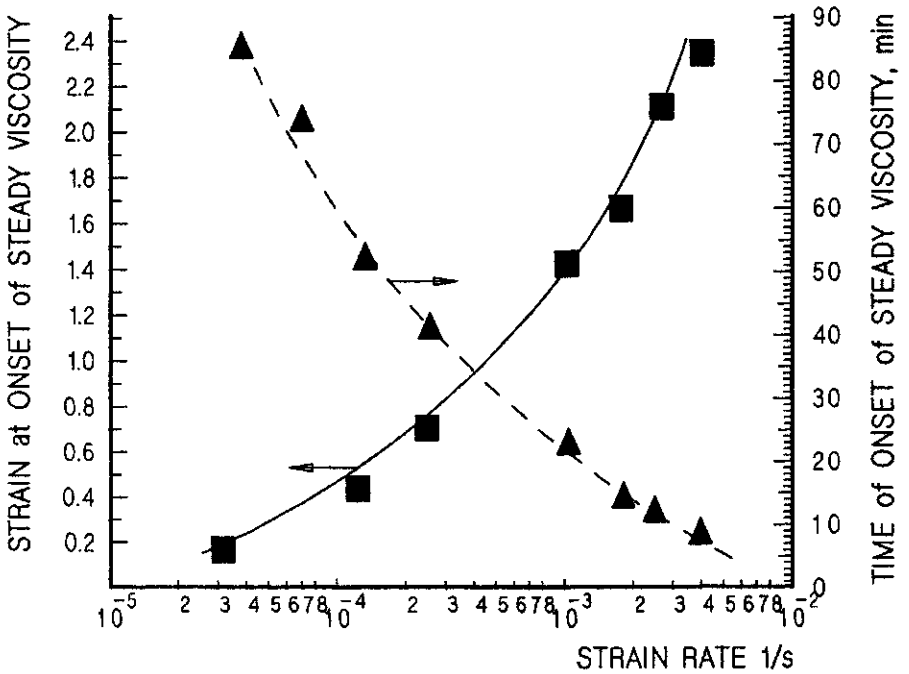

Figure IV.7: *Relationship between extensional viscosity and total strain (bottom), as well as irreversible strain (top). Deformation rates given as parameter. After G. V. Vinogradov and al.*[33]

Extrapolation of all the curves, irrespectively of the deformation rate, down to zero extension gives the Trouton viscosity, ζ_0, which is equal to three times the zero shear viscosity. The extrapolated Trouton viscosity agrees with the relationship proposed by Kargin and Sogol'owa[34]:

$$\zeta = \zeta_0(1 + \varepsilon_i) \tag{IV.34}$$

At low strain rates, viscosity of the constant, strain independent segment is equal to the Trouton viscosity; at higher deformation rates, however, this does not hold true.

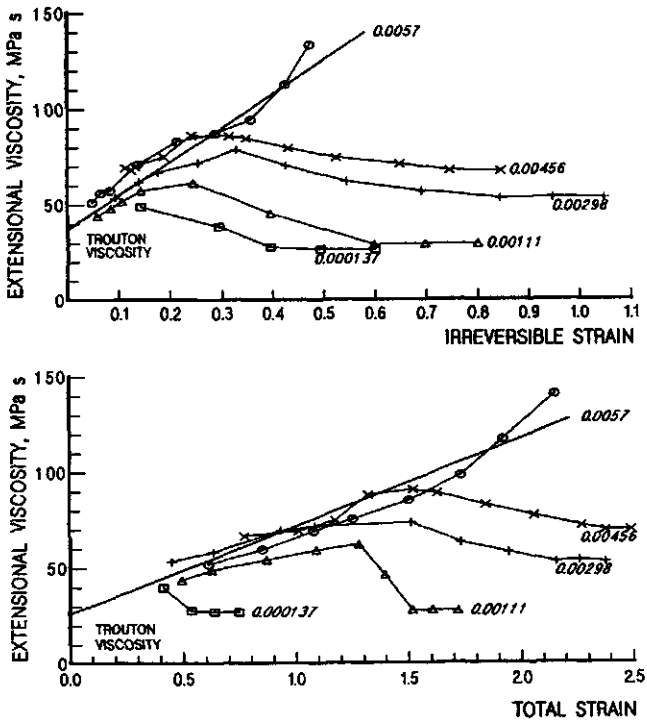

Figure IV.8: *Relationship between extensional viscosity and total strain (bottom), as well as irreversible strain (top). Deformation rates given as parameter. After G. V. Vinogradov et al.*[33]

Modulus of elasticity (figure IV.9) at low extension rates shows some similarity with the corresponding relationship for elongational viscosity. Namely, there is initially a maximum and a plateau, where the modulus does not change with extension. With increasing extension rate, the initial maximum disappears, but there is a segment of extension insensitive modulus. At high extension rates, no region of constant modulus appears before a rupture takes place.

Figure IV.10 and IV.11 show the influence of extension on the stress relaxation, given as $\ln(\sigma/\sigma_0)$ against time. Comparison of the two figures shows the difference in the relaxation behavior between the material stretched at the lowest and the highest deformation rates of those studied by Vinogradov et al.

At this point, a new way for assessment of the relaxation process is introduced: namely, the notion of the *initial time of relaxation*, which is defined as the initial slope of relaxation time versus natural logarithm of the stress decay:

$$\theta_0 = \lim_{t \to \infty} \left[\frac{dt}{d\ ln(\sigma/\sigma_0)} \right] \tag{IV.35}$$

In figure IV.12, the values of so obtained initial time of relaxation are plot-

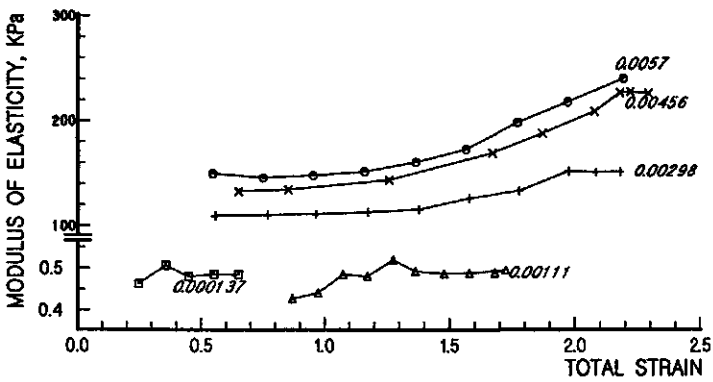

Figure IV.9: *Modulus of elasticity in relation to strain and strain rate (given as parameter). After G. V. Vinogradov et al.*[33]

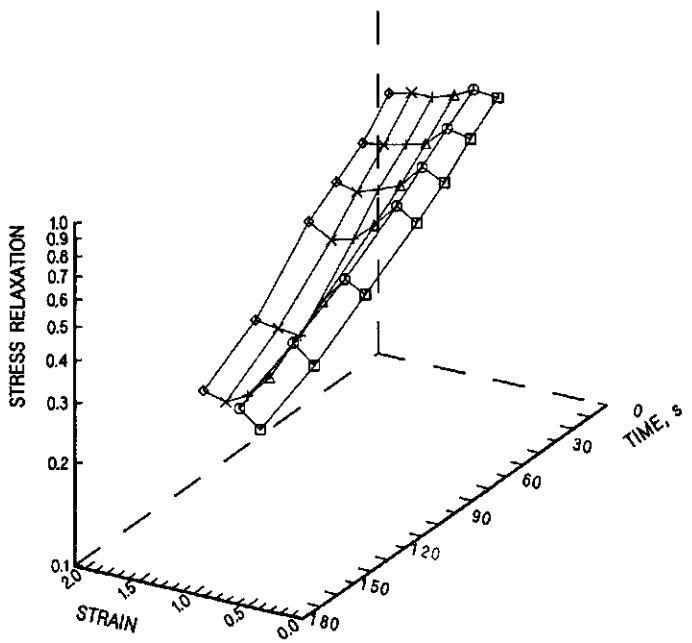

Figure IV.10: *Stress relaxation versus time and strain for extension rate of* $1.11 \cdot 10^{-3} s^{-1}$. *Data from G. V. Vinogradov et al.*[33]

ted against deformation for three deformation rates. It is noteworthy that some of the curves have maxima, and these maxima occur at values of deformation close to those encountered in the relationship between extensional viscosity and

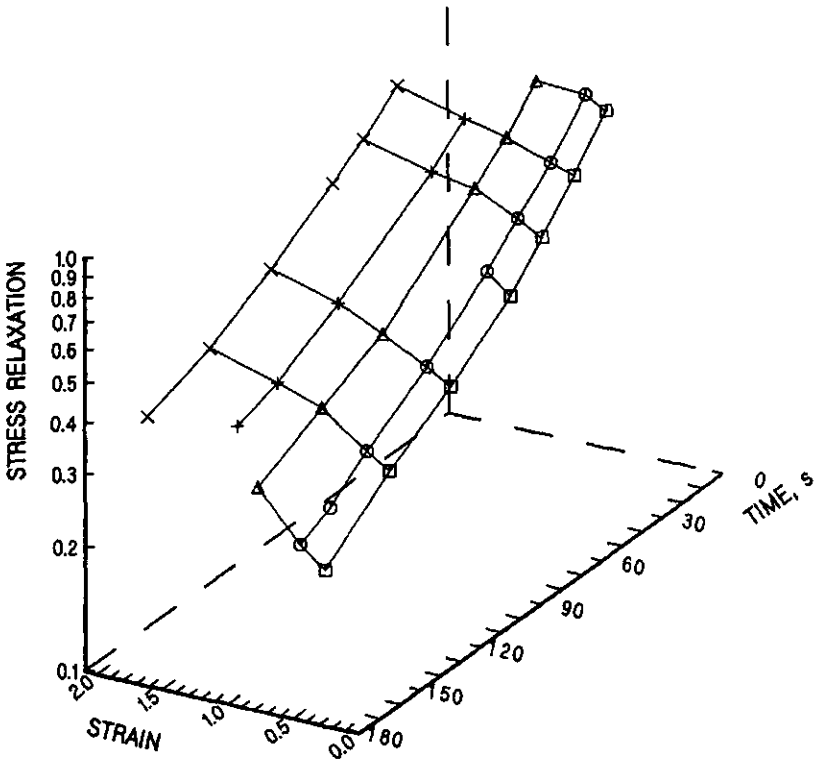

Figure IV.11: *Stress relaxation versus time and strain for extension rate of* $5.7 \cdot 10^{-3} s^{-1}$. *Data from G. V. Vinogradov et al.*[33]

deformation, which are indicated in the figure IV.12 by the arrows.

Although the extensional deformation, as evident from the above quoted results, cannot be treated in a simple Maxwellian fashion characterized by a single relaxation time, but rather with the entire spectrum, the authors use the linear formalism to describe the relation between the stress relaxation after the cessation of extension.

$$\sigma = \varepsilon \int_0^\infty \frac{N(s)}{s} \exp(-\, t\, s)\; ds \tag{IV.36}$$

The function $N(s)$, the *relaxation frequency distribution*, is calculated from $\sigma(t)$ using the first approximation method by Alfrey.[35]

$$N(s) = -\frac{dp}{\varepsilon\, d \ln t} \tag{IV.37}$$

where $s = 1/t$. If the calculations are conducted correctly, then it should result that

$$\int_0^\infty \frac{N\,(s)}{s}\; ds = \;\zeta \tag{IV.38}$$

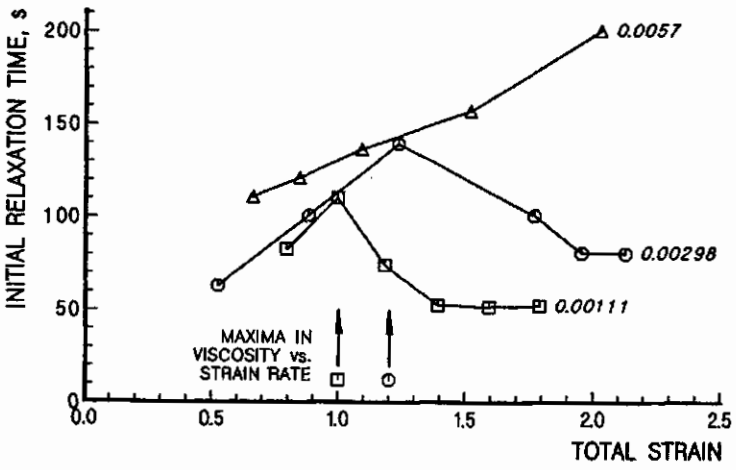

Figure IV.12: *Initial time of relaxation for different levels of strain. Strain rate given as parameter. After G. V. Vinogradov et al.*[33]

If the value of the integral is smaller than ζ, then the spectrum is incomplete.

Figure IV.13 presents the dependence of the relaxation frequency distribution function on frequency and strain in a three dimensional graph. Figure IV.14 gives in the similar form of the three dimensional graph the relationship between the relaxation frequency distribution functions on frequency for constant viscosity flow at different deformation rates.

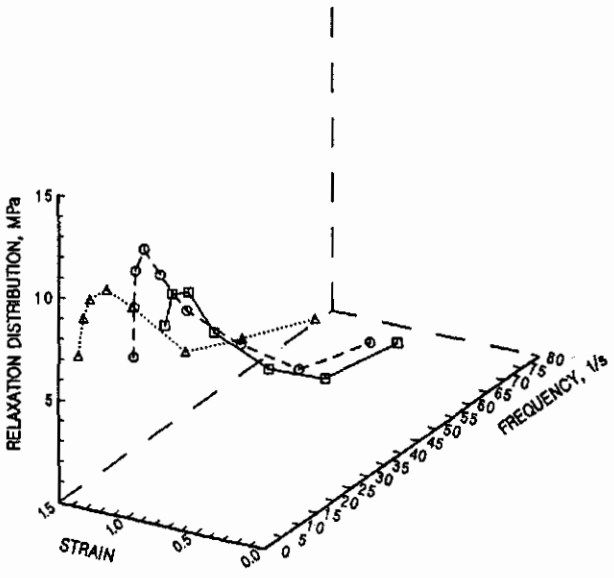

Figure IV.13: *Plot of relaxation frequency distribution in relation to the frequency and to strain. From the data by G. V. Vinogradov and al.*[33]

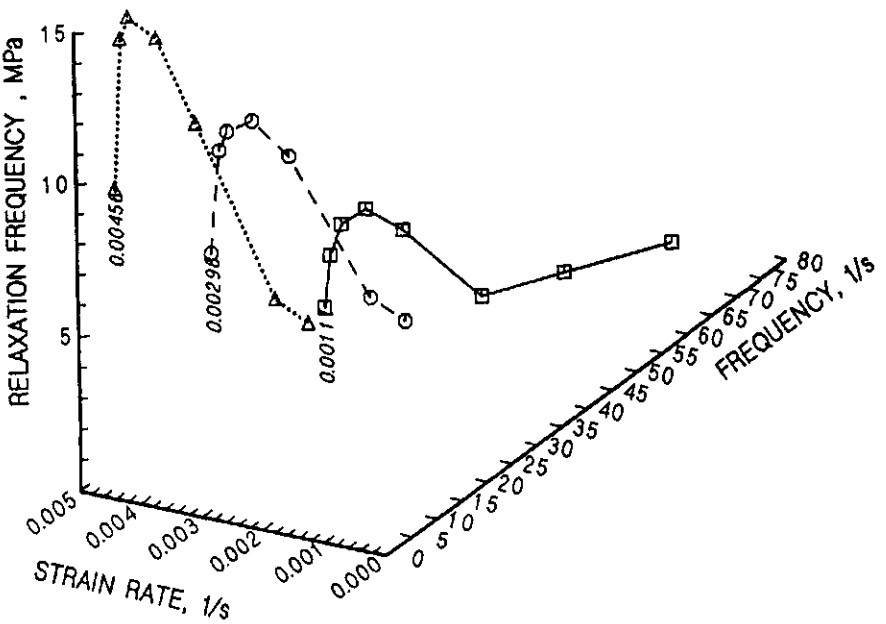

Figure IV.14: *Plot of the relationship between the relaxation frequency distribution and frequency for constant viscosity at different rates of deformation, From the data by G.V. Vinogradov et al..*[33]

Another important result of the investigations by Vinogradov *et al.*[33] is the indication of the strength of polymer in relation to the processing conditions. The molten samples of polystyrene investigated in the extensional rheometer were "instantly" vitrified upon extension and tested for strength. Results of these experiments are shown in figures IV.15 and IV.16, where the rupturing stress is plotted against the total strain (figure IV.15), and the rupturing stress against the irreversible strain (figure IV.16). The arrows in figure IV.15 indicate the values of the total deformation where the maxima of viscosity are reached before a steady state had been reached. Both of the figures witness to the fact that the rate of deformation has a significant effect on the strength of the vitrified samples. This permits also the inference that similar increase of strength regards the melt prior to the vitrification. Vinogradov *et al.* suggest that the increase of strength is primarily due to the increase of reversible, high elastic strain.

In a later publication, G. V. Vinogradov[36] elaborates on the flow instability in extension. According to his findings, a stable extensional flow may be realized as long as stress does not exceed the critical value of 0.1 to $0.5Pa$ – it is the same stress value as is for the shear experiments.

The authors[33] conclude that the total strain (or draw ratio, as it may be expressed) should not be regarded as the parameters determining orientation effect in the polymers. This is in full agreement with similar conclusions reached by other investigators at numerous other occasions. Vinogradov *et al.* emphasize that once the extension process reaches steady state, there is no strength increase any more.

This value is essentially independent from temperature and molecular mass for a given homologous series. It must be noticed, however, that critical shear rate depends on temperature and molecular mass.

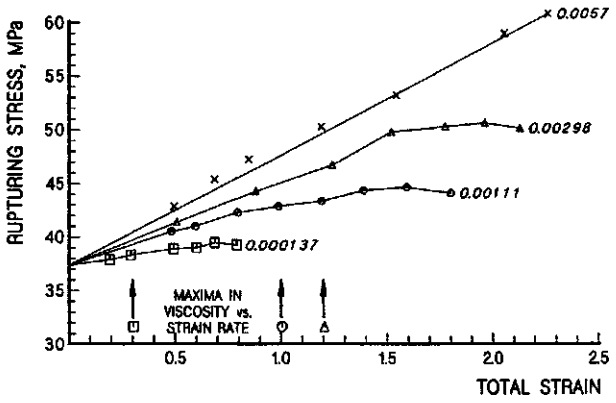

Figure IV.15: *Relationship between the rupturing stress and total strain. Extension rate as parameter. The arrows indicate the deformation at which the maximum of viscosity was attained. After G. V. Vinogradov.*[36]

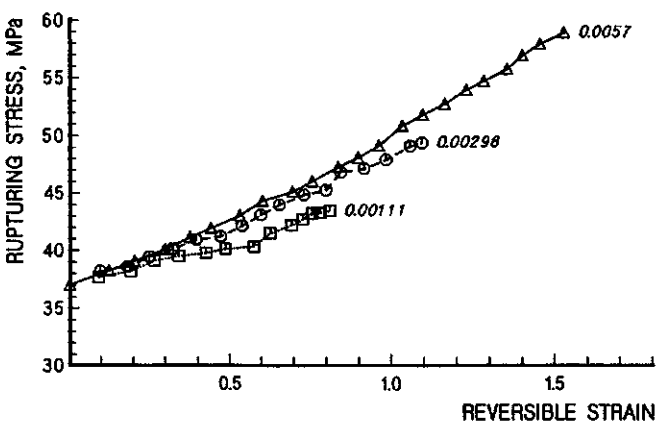

Figure IV.16: *Dependence of tensile strength on reversible strain. Extension rate as parameter. After G. V. Vinogradov.*[36]

At stresses and deformations below their critical values at isothermal conditions, the extensional viscosity remains constant within a reasonably narrow range. Conversely, if the critical values are exceeded, a flow instability may appear. The fact that when the critical stress (or strain) values are exceeded, the ability of polymer to accumulate additional irreversible deformation is reduced can be an explanation for the preceeding statement. On the other hand, the accumulation

of reversible deformation is limited to ultimately reach a level corresponding to its relaxation ability. Consequently, the polymer passes into a forced rubbery state and will start to fracture. In the forced rubbery state, the polymer behaves as a cured elastomer, where an increase of the deformation rate causes the reversible tensile deformation to pass through a maximum, which indicates passing into a glassy state – a state of brittleness.[37]

Other investigators[38–42] find, with substantial theoretical backing, that fractured flow of polymer melts shows significant dependence on extension rate and temperature. With increasing temperature, fracture starts at increasing extension rates. However, with significantly higher extension rates the fracturing disappears. The extension rate at which the fracture disappears increases with decreasing temperature.

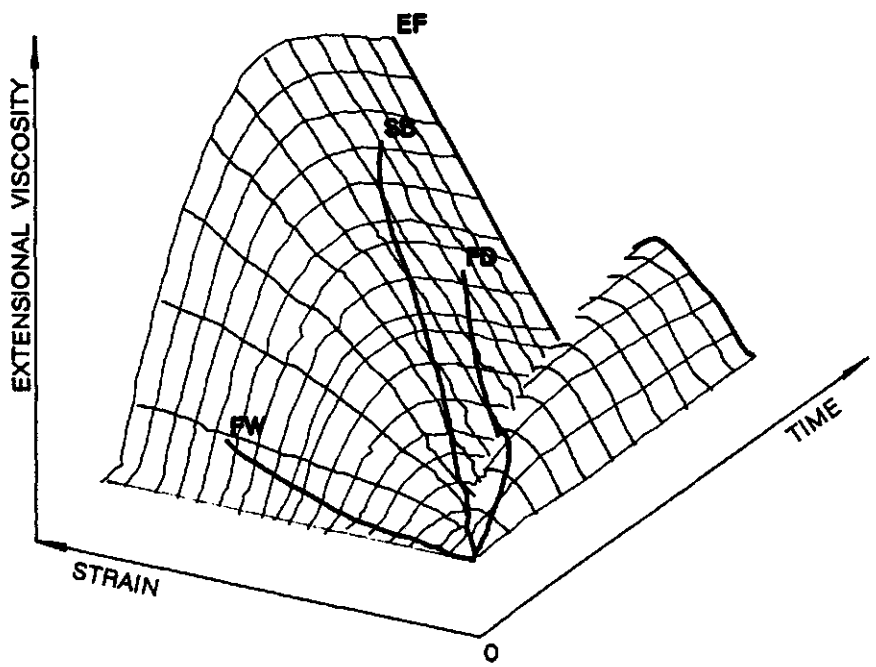

Figure IV.17: *Plot of the transient elongational viscosity as a function of the total strain and time calculated according to Marucci et al.*[43]*. The heavy lines indicate: SB - data calculated from spinning experiment, FD - determinations by the method of falling drop , FW - data calculated with falling weight method. EF - indicates beginning of the steady state (equilibrium) flow. Based on J. Ferguson and N. E. Hudson.*[47]

There is a substantial similarity between the observations by Vinogradov and the graph presented in figure IV.17 which gives a mapping of the transient elongational viscosity *versus* total strain and time.

Thanks to the work by J. Ferguson and N. E. Hudson[47], and naturally to the underlying constitutive equations,[43–46] we have a good visualization of the somewhat "strange" results of the exhaustive experimental studies by Vinogradov et. al.,[33,36] as well as an understanding of the reasons behind the differences in elongational viscosity when measured by different techniques. It would be interesting to determine how the results of the determinations of elongational flow in hyperboloid cone orifices[136,137] would compare with the other data of figure IV.17. The work of Ferguson and Hudson[47] also gives additional explanation of the transient shear flows discussed by Vinogradov.

It is important to realize that the majority of the experimental techniques for the determination of elongational viscosity, as well as the majority of industrial processes involve only the transient flow region. Undoubtedly, this creates a difficult situation if there is a necessity to relate laboratory analyses with the material behavior in any industrial process.

Phan-Thien and Tanner[48,49] have developed another linear model, with additional improvements over the model of Marucci *et al.*[43]. Additionally, the model does accommodate nonisothermal cases:

$$\mathcal{T} = \sum_{i=1} \mathcal{T}^{(i)}$$

$$\theta_i \frac{D}{Dt}\mathcal{T}^{(i)} - \mathcal{T}^{(i)}\frac{\mathrm{d}}{\mathrm{dt}}(\ln \mathrm{T}) = \phi(\mathrm{T})\ \mathrm{K}(\mathrm{tr}\mathcal{T}^{(i)}\ \mathcal{T}^{(i)} = 2\ \mathrm{G_i}\ \theta_i\ \mathrm{D} \qquad \text{(IV.39)}$$

where

$$\phi(T) = \exp\left[\frac{c_1\ (T - T_r)}{c_2 + T - T_r}\right]$$

which represents the exponent of the inverse of WLF equation,

$$K(tr\mathcal{T}^{(i)} = \exp\left[\frac{\epsilon}{\mathrm{G_i}}\ \mathrm{tr}\ \mathcal{T}^{(i)}\right] \qquad \text{(IV.40)}$$

ϵ is a constant on the order of 0.01, D is stretching tensor, $\mathcal{T}$ is stress tensor, θ is relaxation time, G is modulus, and $G_1 = G\ H\ (1 - \xi)$, where H is relaxation function, and ξ is an adjustable parameter. Further,

$$\frac{D\,\mathcal{T}}{D\,t} = \frac{d\,\mathcal{T}}{d\,t} - \mathcal{L}\,\mathcal{T} - \mathcal{T}\,\mathcal{L}^{\mathrm{T}}$$

with L, the macroscopic velocity gradient and $\mathcal{L} = \mathrm{L} - \xi\ \mathrm{D}$, and finally $tr\mathcal{T} = [3\mathrm{kT}/(\mathrm{N}\alpha^2)] \cdot \langle\lambda\rangle^2$, and $\langle\lambda\rangle^2$ is mean square extension of the molecular entanglement network strand.

The just given constitutive equation has been adapted for application to the fiber formation problem[49], giving the following set of equations:

$$K\mathbf{T}_i + \alpha_i\left\{u\frac{d\ \mathbf{T}_i}{d\ m} - 2\ (1 - \xi)\frac{d\ u}{d\ m}\mathbf{T}_i\right\} = 2\ \alpha_i\ \frac{d\ u}{d\ m} \qquad \text{(IV.41)}$$

$$K\mathbf{P}_i + \alpha_i \left\{ u \frac{d\,\mathbf{P}_i}{d\,m} - (1-\xi)\frac{d\,u}{d\,m}\mathbf{P}_i \right\} = -\alpha_i \frac{d\,u}{d\,m} \tag{IV.42}$$

$$\sum_{i=1}^{N} \frac{\epsilon_i}{\alpha_i} \; (\mathbf{T}_i - \mathbf{P}_i) = u \tag{IV.43}$$

where $\alpha_i = \theta_i v_0 / L$ is Deborah number and $\epsilon_i = G_i\, \theta_i\, Q \;/\; F\, L$ but $\epsilon_i/\alpha_i = \phi_i$. The boundary conditions are given as:

$$z = 0, \qquad u = 1, \qquad \text{and} \qquad \sum_{i=1}^{N} \phi(bfT_i - \mathbf{P}_i) = 1$$

It is stipulated that the initial stress distribution does not affect the solution over the entire fiber path. This is the result of an assumption that at $z = 0$ $\mathbf{P}_i = 0$ and $\mathbf{T}_i = 1/N\phi_k$.

The final version of the equations for a fiber formation case is:

$$\sum_{k=1}^{N} \phi_k(\mathbf{T}_k - \mathbf{P}_k)\frac{d\,\mathbf{T}_i}{d\,m} = 2\,\Xi\,[1 + (1-\xi)\mathbf{T}_i] - \frac{K}{\alpha_i}\mathbf{T}_i \tag{IV.44}$$

$$\sum_{k=1}^{N} \phi_k(\mathbf{T}_k - \mathbf{P}_k)\frac{d\,\mathbf{P}_i}{d\,m} = -\Xi\,[1 + (1-\xi)\mathbf{P}_i] - \frac{K}{\alpha_i}\mathbf{P}_i \tag{IV.45}$$

where

$$\Xi = \frac{\sum\limits_{i=1}^{N} \phi_i/\alpha_i \; K(\mathbf{T}_i - \mathbf{P}_i)}{\sum\limits_{i=1}^{N} \phi_i \,[(1-2\,\xi)\mathbf{T}_i + \xi\,\mathbf{P}_i] + 3\sum\limits_{i=1}^{N} \phi_i} \tag{IV.46}$$

Equations IV.44 to IV.46 present a set of first order differential equations. The needed input is take-up force, initial velocity, and flow rate. In terms of analytical preparations, full rotational and oscillatory determinations are needed. Also, very crucial is the knowledge of the relaxation function, though the author does not specify what type of relaxation and this segment of the work raises some questions. Solution of this set of equations gives stress distribution along the spinline, velocity profile and draw ratio. The draw ratio, if known, cannot be specified independently.

Phan-Thien[49] presents a test of the validity of the equation on data obtained for formation of fibers from low density polyethylene[50] and polystyrene,[51] both noncrystallizable polymers. The formation processes were very slow, far from the industrial level of intensity. The agreement between the calculated results and the data measured from the experiment are much better than any of those published earlier. Nevertheless, the discrepancies grow with the growing distance from spinnerette, similarly like in many other publications, to reach some ten to fourteen per cent. One must admit that the calculations are quite involved, as is the analytical preparation.

Several authors concede that solution of the "spinning problem" by way of the constitutional equations developed thus far is essentially unsuccessful.[24,139–142]

IV.4.c Andigraphic Solution of Attenuation

Another way of resolving the "spinning problem" is offered by this author in the framework of a complex treatment of all the unit processes taking place in the quench zone.

When one considers a process with constant take-up force, then the force acting on any cross section along the spin line is constant, in the first approximation. The differences in force level are caused only by "the losses to the environment", etc. Additionally, as the polymer stream emerges from the exit of the spinnerette, it is subjected to a drawing force which may be understood as a case of step stress excitation. The force superimposes on the effects of the forces applied earlier in the extrusion process. The step application of force is a precondition for the qualification of a process as *creep*. After scrupulous examination of all kinds of analytical data collected on many different fiber formation processes, we find that they do not resemble extensional rheometric data or plots. With this in mind, in addition to the lack of real success in describing the process by all means tried thus far, it has been assumed that the process of diameter attenuation in fiber formation is a process of *creep*. As the additional justification for such an assumption, it may be given that in the course of attenuation, there is no qualitative difference between fiber formation with constant take-up velocity and constant take-up force. This is the matter of long recognized *"self regulation"* of the mutually interdependent quench zone processes. In a drawing process, *e.g.* during rheometer testing, the extension of the material is by definition under strain excitation, the diameter reduction is uniform over its entire length, while the extending force increases with the growing strain. In reality, in fiber formation this is not the case, despite the fact that in fiber makers' slang the operation is called *melt drawing*. K. Katayama, T. Amano, and K. Nakamura[63] quite long time ago observed during formation of fibers from polyethylene that diameter attenuation fits into the Kelvin-Voigt model, a model describing creep.

Figure IV.18 presents the apparent extensional viscosity and strain plotted against time. The data were taken from the detailed analyses of several medium fast industrial processes, and they span from the maximum of the die swell to the end of crystallization. All of the cases presented in figure IV.18 show very distinct similarity: the extensional viscosity (non-isothermal, as it is in the process) is practically constant at a very high level, possibly with a slight negative slope. According to Vinogradov, [33,36] this should be an indication of linearity of the system. Naturally, it is to be expected that shortly before the initiation of crystallization some kind of "havoc" takes place in the polymer morphology. One cannot expect to describe adequately this segment of polymer history by a linear relationship.

On the basis of the above assumptions, the empirical data may be used to calculate creep compliance as a function of time. From such a relationship one

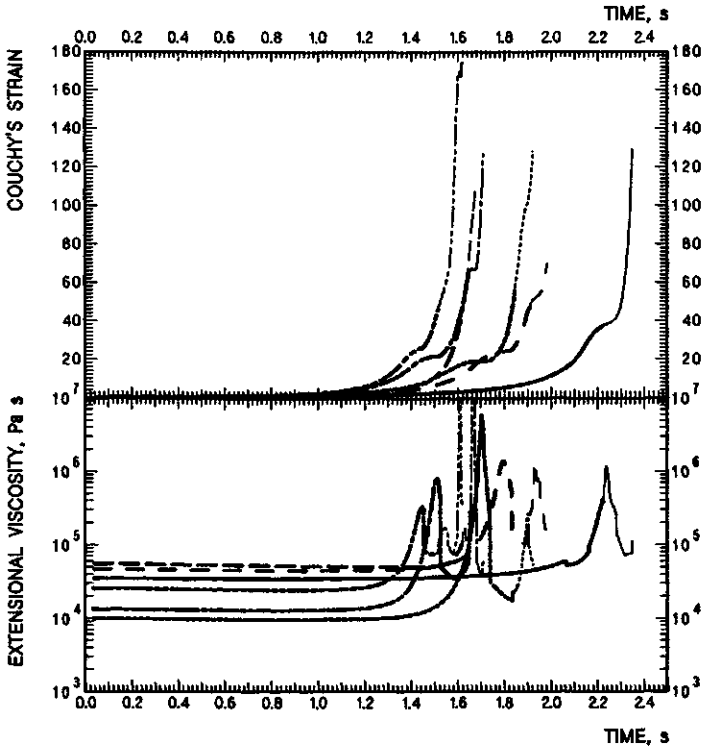

Figure IV.18: *Apparent extensional viscosity and strain obtained from analysis of several medium fast industrial processes of fiber formation. The time scale spans from the maximum of the die swell to the onset of crystallization. Polymer: polypropylene. Nonisothermal, "as is" data given.*

may calculate retardation distribution function which represents the essence of viscoelasticity and permits to depict all pertinent rheological functions: thus the title "andigraphic", from $\alpha\nu\tau\iota\gamma\rho\alpha\phi\phi\nu$ = depiction, image, reflection.

There are several methods available for calculations of the relaxation and retardation spectra.[31] The finite difference operator approximation method by Yasuda, Ninomiya, and Tschoegl[32] appears to be accurate and convenient, provided that the third order approximation equation is used. The needed equation is given as:

$$L(\theta/\beta^*) = \frac{J(h^3\,t) - (h^2+h+1)\;J(h^2\,t)}{(h^2-1)(h-1)\;\ln\;h} + \\ + \frac{h(h^2+h+1)\;J(t) - h^3\;J(t)}{(h^2-1)(h-1)\;\ln\;h}\Bigg|_{t=\theta} \qquad \text{(IV.47)}$$

The notation here is: L – creep retardation spectrum, t – time, θ – retardation time, h – finite difference time increment, β^* – spectral shift factor given for several $\log h$ values in table IV.1. Time is commonly used in a logarithmic scale and so

is the time increment. Following Tschoegl's[32] notation in equation IV.47 ht really means $\log t + \log\ h$ and $h^2 t$ corresponds to $\log t + 2\log h$ etc. The value of h is usually selected so that its logarithm equals between 0.1 and 0.5. With decreasing value of h, the accuracy of the spectra increases but with $h < 0.1$ the sensitivity to error in the input data greatly increases, and this may eventually lead to increased uncertainty of the obtained retardation function.

Table IV.1.
Spectral shift for various finite differences for third order approximation. After N. W. Tschoegl[31]

$\log h$	0.1	0.2	0.3	0.4	0.5
β^*	2.139	1.550	1.150	0.878	0.689

Once we have a retardation function, almost everything else may be calculated. The suggested way of process description is accurate. The retardation function is strongly affected by deviations in polymer chain structure and the suggested procedure provides data for the polymer one works with. There are, however, several points to be observed.

According to Stavermann and Schwartzl[52], the process of creep is inherently nonlinear. Following J. Marin[*cit.in* 52] creep is customarily interpreted as consisting of three parts:

1. Instantaneous creep, ε_0;
2. Transient creep, $[\varepsilon(t)]$, which increases with time from zero to some finite equilibrium value;
3. Steady state creep, $[\phi_f \cdot t]$, proportional to time (see Figures IV.19 and IV.20).

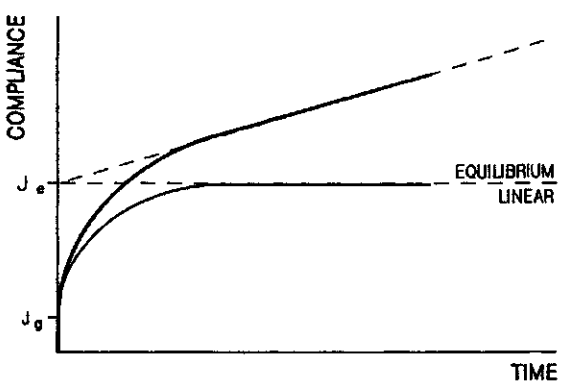

Figure IV.19: *Generalized schematic representation of compliance (or strain) versus time in response to step application of stress: creep behavior.*

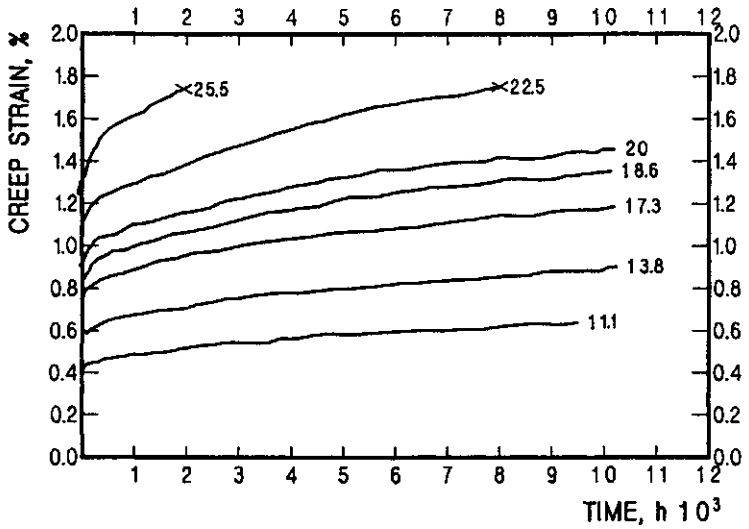

Figure IV.20: *Extensional creep of polymethyl methacrylate; parameter: initial stress in MPa. After J. Marin*[cit.in52]

The marks "linear" or "equilibrium" in figure IV.19 represent the strictly linear creep. The instant compliance (strain) is a nonlinear feature. The same is true of the steady state fluidity, $\phi_f \cdot t$, in figure IV.19 represented by the triangle contained between the lines tangent to the equilibrium compliance (dashed lines) and the full, measured compliance. The angle ϕ_f represents the rate of steady state fluidity increase.

If very large forces are applied, some "additional nonlinearities" in the creep behavior may be observed. In such cases one may escape to linearization of the data.[52] Linearization of rheological functions is easiest and correctly done by application of various definitions of strain.

According to K. Weissenberg[53], any function of the shape of the body which vanishes when the body is undeformed and which increases with increasing deformation may be used as a measure of strain. According to A. J. Stavermann and F. Schwartzl[52], the various commonly used definitions of strain are:

$$\varepsilon_C = \delta - 1 \qquad \textit{Cauchy} \qquad \text{(IV.48)}$$

$$\varepsilon_K = 0.5(\delta^2 - 1) \qquad \textit{Kirchhoff} \qquad \text{(IV.49)}$$

$$\varepsilon_H = \ln \delta \qquad \textit{Hencky} \qquad \text{(IV.50)}$$

$$\varepsilon_M = 0.5\left(1 - \frac{1}{\delta^2}\right) \qquad \textit{Murnaghan} \qquad \text{(IV.51)}$$

where $\delta = \frac{l}{l_0}$ which is equivalent to *draw ratio.*

Cauchy's strain is linear with the value of delta, Kirchhoff's strain in relation to Cauchy's increases with increasing delta. The remaining two functions, in relation

to Cauchy's, decrease with increasing delta, but Murnaghan's strain has a stronger decrease, its maximum limiting value is 0.5. Zero point, naturally, is common for all of the quoted definitions of strain.

When one calculates creep compliance, one uses, naturally, the initial stress and any of the given quoted strains. Murnaghan's strain needs to be used for industrial fiber formation processes at high speed and under high tension. For slower processes Hencky's strain may be sufficient. Cauchy's strain, possibly, may be applicable for very slow experimental ("academic") processes. Equation IV.47 may be used with any of the strains, but one must remember to recalculate the results into Cauchy's strain for use in generating other functions.

Generally, equation IV.47 ought to be applied to the experimental data with a correction for the transition from shear to extensional flow. The problem has been worked on by many different authors. The more interesting experimental work appears to be that by J. R. Clermont, J. M. Pierrad, and O. Scrivener,[56] and D. D. Goulden and W. C. MacSporran.[57] Attempts on a theoretical solution may be represented by work of R. Keunings, M. J. Crochet, and M. M. Denn.[58] The solutions offered do not seem to be quite yet ready for practical application.

Measurement of the maximum diameter of the die swell is somewhat elusive, as it also depends markedly on the deformation history. On industrial formation machines measurements of the die swell are very difficult due to deep recess in mounting of the spinnerettes, often the access in impossible. The diameter, or the related filament velocity, is needed for calculation of strain. If there is an error in the die swell size it will automatically propagate an error in the time scale. It seems that when the correct theoretical solution of the flow transition will be known, obtaining correct data on die swell may be easier.

The beginning of the attenuation process is usually considered to be at the maximum of the die swell diameter. For the representation of the creep curve, however, it is necessary to push the *zero time* back to the point where polymer enters the conical entrance to the capillary. This means that the *zero time* is where the extensional flow starts first. In this way the *zero time*, in comparison with the common notion of maximum of die swell, depends on the entire geometry of the capillary entry, on the length of the spinnerette capillary, as well as on the size and shape of the die swell.

The back calculation of compliance, J, or strain, with the retardation distribution function, L, on hand may be done with equation III.140. Nonetheless, there are also necessary the instantaneous compliance. J_0, and the steady state fluidity function, ϕ_f. In a classic way, one obtains those two values by the method shown in figure IV.19. This means that, J_0 - equals instantaneous compliance at time zero. The slope of the final section of the curve, ϕ_f, is usually taken as the steady state fluidity, $\phi_f(t)$.

The compliance back calculated from the retardation function represents only the transient flow portion, $J(t)$. The steady state fluidity in more intensive fiber formation processes for large strains deviates from linearity at longer times, t. Therefore, the procedure of calculating instantaneous compliance and steady state

fluidity must be modified. The transient flow compliance, as it is calculated from the retardation function, is subtracted from the experimental compliance over no more than a 50% of the time span of the process studied. One may also begin the calculations at some distance from the first point available. The obtained values *versus* time give a new function which represents a straight line, the slope of which determines the steady state fluidity, ϕ_f, and J_g is the intercept. In case of processes involving large strains the experimental curve at longer times invariably deviates from linearity, The process gradually changes from rheodictic to *pseudo-arrheodictic* behavior. The experimental compliance curve ceases to increase and reaches a more or less constant value which is typical for the arrheodictic behavior. The point where the steady state fluidity begins to deviate from linearity depends on the molecular mass of the polymer involved, as shown in figure IV.21. The molecular mass influence is likely to be rather indirect, caused really by the density and type of deep entanglements, or enchainments. One may want to fit the final segment of the curve into some nonlinear function, usually $\phi_f^*(t) = 1 - A \times \exp(ct)$. Such a treatment may improve the fit of the back calculated results to the point of virtual superposition of the experimental and back calculated curves. One may use one of the solutions suggested by Tschoegl[156], though some of them require data not easily available. The most suitable might seem the *prolongation method*, however, the method appears to be much more manipulative than the curve correction suggested above. It is true that the span of retardation times obtainable is very narrow but alteration of the spectrum seems objectionable. According to Tschoegl[156] the pseudo-arrheodictic behavior results from *pseudo-crosslinks* arising from strong and relatively durable entanglements, which are responsible for more than one viscoelastic mechanism reflected by multimodal distribution function. The data presented here may suggest that the observable effect of the pseudo-crosslinks is reflected by change of the steady state fluidity, rather than the transient flow reflected by the retardation spectrum. As it will be seen later in this chapter, the arrheodictic behavior is the "havoc in morphology" of the melt prior to the onset of crystallization. If long retardation times would be involved, they would be significantly longer than the times available in any fiber formation process.

Here we come to the temperature dependence: currently all of the formation processes from melt are nonisothermal, and so are many processes of formation from solution. There is a wide choice of recalculation possibilities according to temperature.[32,33,54,55] One may recalculate compliance according to (the same equation as III.219):

$$J(T_r, t_r) = J(T, a \cdot t_r) \times \left(\frac{\rho\, T}{\rho_r\, T_r} \right) \tag{IV.52}$$

where subscript r indicates reference temperature or at reference temperature, a is temperature-time shift factor, ρ is polymer density.† The retardation distribution

†Data on certain physical properties of some polymers are given in the Appendix.

function may be recalculated identically as compliance.

$$L(T_r, t_r) = L(T, a \cdot t_r) \times \left(\frac{\rho\, T}{\rho_r\, T_r} \right) \qquad (IV.52\,a)$$

The shift factor may be estimated either according to the equation III.217 or equation III.220 for polypropylene. For other polymers development of similar algorithms is highly advisable. Application of the recalculation procedures may be done in several different ways, or at several different stages. The two most obvious ways are:

1. Recalculation of compliance, and obtaining the retardation spectra for non-isothermal and for isothermal conditions separately.

2. Recalculation of the retardation function.

The first method of the two appears marginally more convenient. Nevertheless, the recalculation must be taken as an approximate procedure, as it has been developed for polymers of linear behavior. The extremely high viscosity immediately below the spinnerette is striking; one may simply presume that this is somehow connected with the transition from shear to extensional flow. We may recall one more time the comment by Stavermann and Schwartzl that creep is by its nature nonlinear; it may be that the degree of nonlinearity is *artificially increased by the process itself.* Even though the function of the shift factor *a versus* temperature, as suggested here, appears to give results sufficiently good for "technical applications", it might require a firm proof in a theoretical sense. Also, the recalculation is obviously only as good as reliable is the available shift factor – temperature function, and the whole function is needed for the purpose. Moreover, the regions where polymers crystallize always require an extrapolation.

All the isothermal compliance curves quoted here were recalculated to $240°C$. These curves show very rapid decrease of compliance at the end of the curve.
]

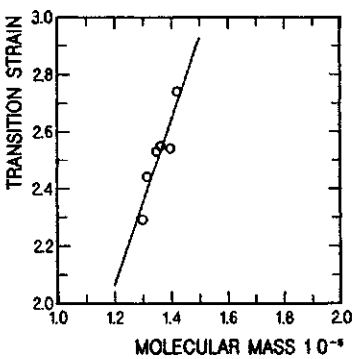

Figure IV.21: *Influence of molecular mass on the strain at which the behavior of polymer in creep changes to arrheodictic.*

One may pose a question whether this means that in an isothermal process such behavior would indicate an end of "spinnability".

Examples of practical application of the description of the rheology of fiber formation processes and confrontation of the calculated results with the experimental are given in the set of figures IV.22, IV.23, IV.24 and IV.25, pertaining to different industrial processes.

A comparison of the two processes represented in Figures IV.22 through IV.24 involves poly(propylenes) of zero shear viscosity 193.6 and 148.8 Pas at $240°C$. The second process was carried out with a substantially shorter quench zone, geometrically speaking, and with a greatly more intensive quench. The initial drawing stresses were 16.97 and 18.73 kPa, respectively.

It is important to stress that the magnitude of the force applied for drawing has a major influence on the creep process. The explanation of rheology through chain entanglements[135] does justify the influence of initial force on the creep process, but more development work seems to be needed before a practical application might be possible. As may be seen from Figures IV.23 and IV.24, primarily the instantaneous strain and steady state fluidity are affected. The steady state fluidity is influenced to a smaller degree, but at higher values of force the behavior is changing to arrheodictic, as mentioned above. From the work presented here one may see an influence of the initial stress on compliance and on the retardation function (figure IV.25). At lower initial stresses compliance is higher and it finds also a reflection in the retardation functions.

Vinogradov and co-workers,[33] as reported in section IV.4.b, figures IV.10 to IV.12, and particularly IV.13 and IV.14 suggest that the retardation function does not depend only on molecular mass or zero shear viscosity, but appears to depend also on the processing conditions. Both theoretical and experimental investigations[155&ref.] indicate with ever increasing strength that relaxation time, or relaxation spectrum, is not constant. In the case of solutions, irrespectively of solvent, it depends on the deformation rate. The influence of initial stress on compliance may be taken as a proven fact, though no quantitative description is yet available.

There is a number of formulas to calculate relaxation time, proposed by different authors.[32,152] All of the proposed equations are similar, the core of the equations is:

$$\theta = \frac{\eta_0}{RT} \tag{IV.53}$$

The retardation times, taken as the time corresponding to the maximum of the retardation spectrum determined for each of the processes studied and quoted here, range from about 0.35 s to about 0.52 s. These times differ substantially from the average relaxation and retardation times determined from the oscillatory shear experiments, where they range from 0.49 s to 0.73 s. The difference appears to be too large to be disregarded. The experimentally obtained retardation times agree well with the results of calculations according equation IV.53a. If a polymer contains cross linked material, the relaxation time increases. A similar effect may be expected in case of retardation time. Cross linking, often present in com-

mercial polymers elevates the relaxation time markedly. In fact, determination of relaxation time may serve, after a calibration, as an analytical procedure for the

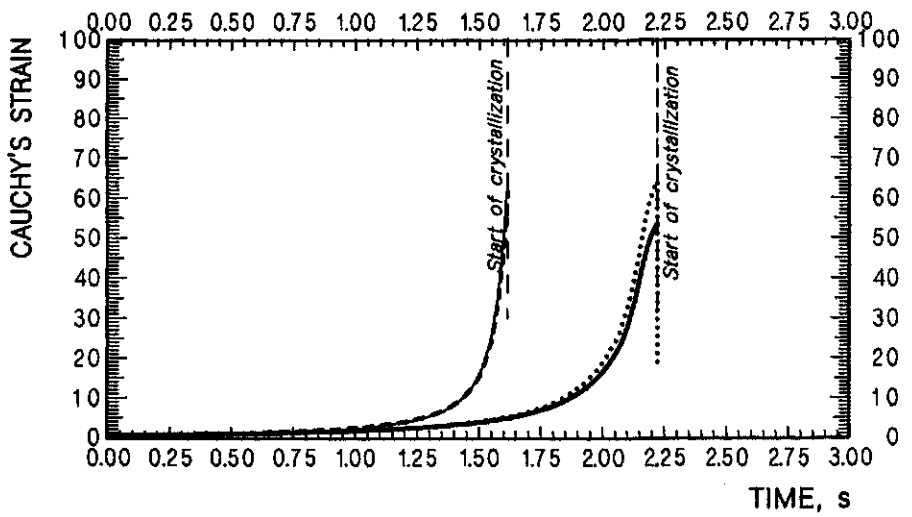

Figure IV.22: *Cauchy's strain in a fiber formation. The dotted line is back calculated. Heavy lines: nonisothermal data for a process with rapid quench, the pseudo-arrheodictic segment not corrected for. Finer lines: process at still more rapid quench, polymer of lower viscosity. Data corrected for the pseudo-arrheodictic flow segment.*

determination of cross linking. The creep retardation times for the polymers given in this chapter as examples are plotted in figure IV.26 against the corresponding

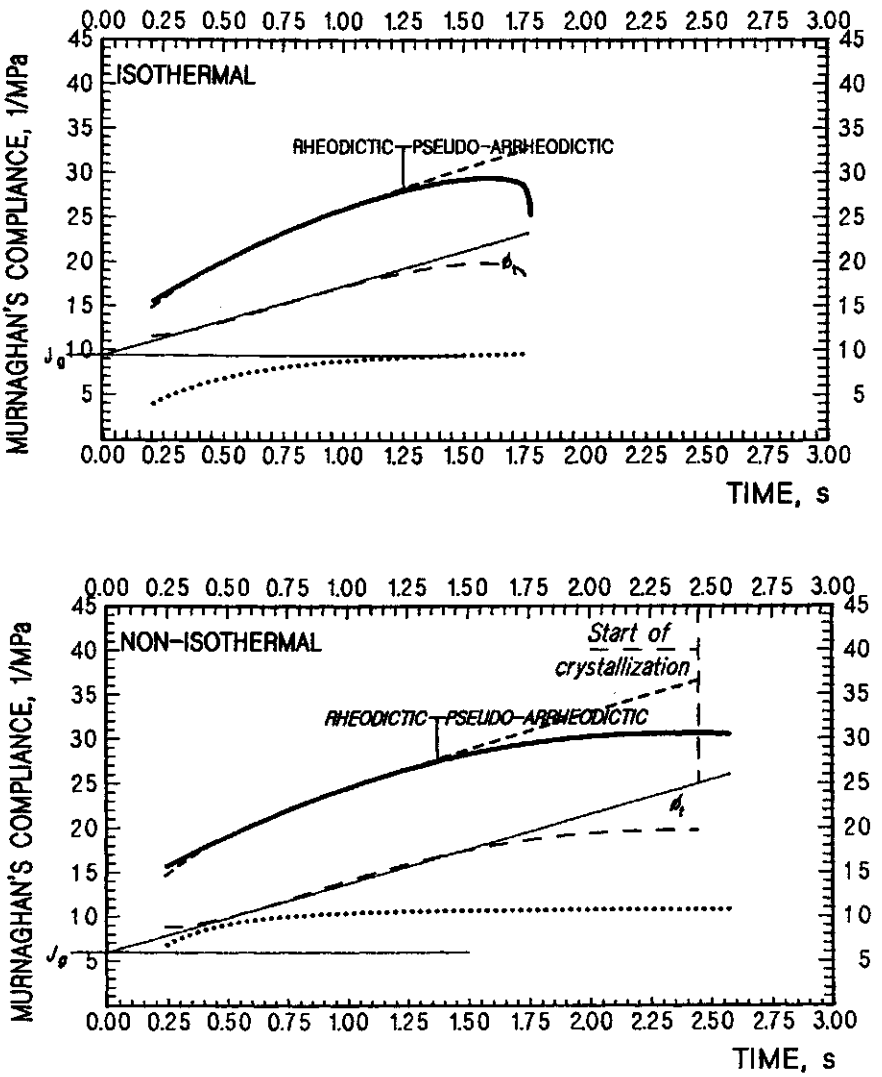

Figure IV.23: *Murnaghan compliance for the process given in Figure IV.22, heavy lines. Top: isothermal, bottom: non-isothermal. Heavy lines: full drawn – experimental curve, dotted – transient flow compliance, short dashed line – back calculated compliance (mostly superimposed with the experimental line). Fine lines: full drawn – linear steady state fluidity, ϕ_t, and glassy (instantaneous) compliance, J_g (intercept), long dashed – actual fluidity. Data not corrected for pseudo-arrheodictic behavior.*

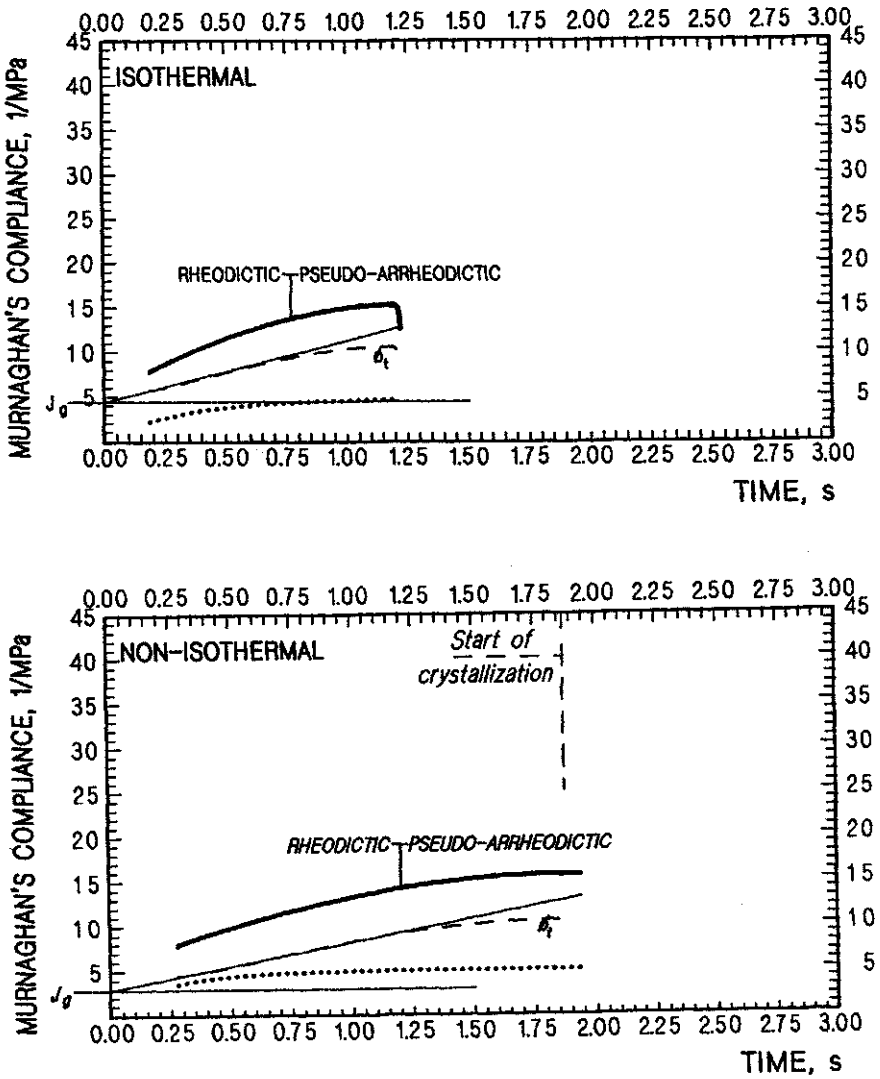

Figure IV.24: *Murnaghan compliance for the process given in Figure IV.22, finer lines. Top: isothermal, bottom: nonisothermal. Heavy lines: full drawn – experimental curve, dotted – transient flow compliance, short dashed line – back calculated compliance (fully superimposed with the experimental line). Fine lines: full drawn – linear steady state fluidity, ϕ_t, and glassy (instantaneous) compliance, J_g (intercept), long dashed – actual fluidity. Data corrected for pseudo-arrheodictic behavior.*

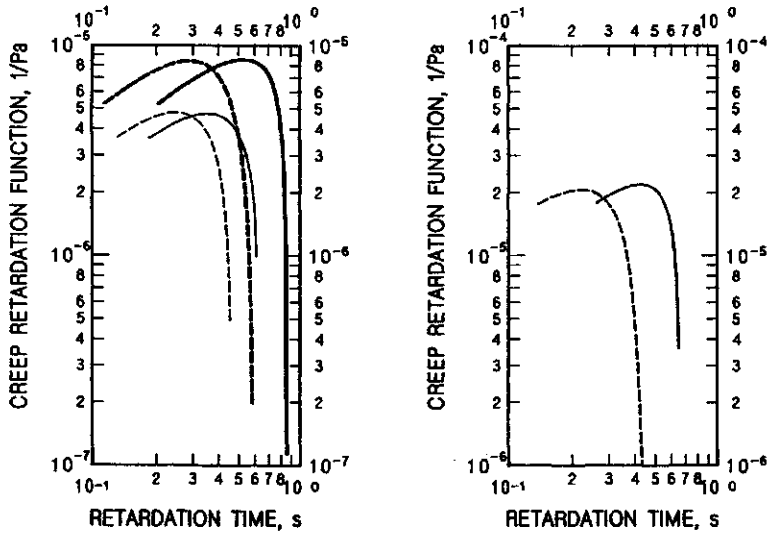

Figure IV.25: *Creep retardation functions: Left graph: for the process given in figure IV.23. Right graph: for the process given in figure IV.24. Full drawn lines – isothermal* $T_r = 240°C$, *dashed lines – nonisothermal.*

values calculated according to equation IV.53a. The deviations of the experimental results from the calculated line do not form any immediately apparent relationship to the initial extensional stress.

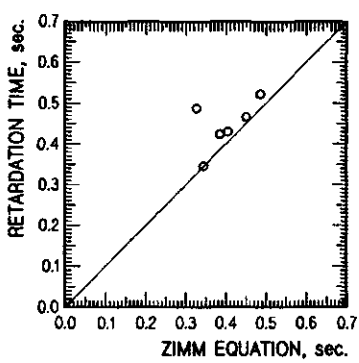

Figure IV.26: *Confrontation of the retardation times calculated from the Zimm equation (equation IV.53a is represented by the diagonal line) with the values determined experimentally. Data for* $240°C$.

$$\theta = \left(\frac{1}{1.8926}\right) \times \left(\frac{\eta_0 M_w}{\rho RT}\right) \qquad (IV.53\,a)$$

Based on the results of the creep calculations described above any relationship between the initial stress and retardation time may not be confirmed. Perhaps the high speed of the processes, and consequently the small range of retardation

times obtainable do not permit such a relationship to be observed.

It may also be necessary to assess the extent to which the data obtained in one process may be used to process manipulations. If the attempted changes in the conditions of formation are large, and if a correction accounting for the initial stress fails, at some point the retardation function may loose its validity even for approximate predictions; a new determination of the retardation function may be needed.

In general, from an analysis of the results, one may conclude that the treatment of the *fiber formation problem as a creep process* is correct. The agreement of the calculated data with the measurements conducted during actual experiments is excellent. The small span of time obtainable for the retardation spectra was initially of a serious concern. However, the results and their good agreement with experiments seem to dispel the fear. The pseudo-arrheodictic segment of the process appears to be related to the polymer fluidity, rather than to the retardation spectrum. The process takes only a very short time and the longer retardation time cannot play terribly significant role here. At some 0.5 s to 0.8 s the retardation functions drop quite precipitously off. If the retardation function were responsibly for the pseudo-arrheodictic behavior then a second peak would be necessary. Attempts to use the prolongation method indicated that to explain the pseudo-arrheodictic behavior observed experimentally would require retardation time unrealisticly long, compared to the time available in the process. The filaments are under tension during all the solidification process and beyond, and this may be the important factor to be considered here.

IV.4.d Spinline Stability

Stability of spinline represents an enormously important aspect of the economy of fiber manufacturing. It is not less interesting theoretically. It is of no surprise, then, that theoretical work on the subject started relatively early by J. R. A. Pearson and co-workers.[59–62] As a starting point, isothermal cases of Newtonian fluids were studied. It has been found that such fluids may be extended to a maximum draw ratio of 20.218. The effort appeared to be a good beginning for further studies. The isothermal spinning of Newtonian fluids *per se* has little practical meaning.

Unfortunately, the subsequent years have brought a score of publications repeating essentially the same work using slight modifications of the mathematical apparatus used. C. J. S. Petrie gives a quite extensive review of all those efforts.[24]

There appeared several attempts to describe stability of spinlines of Non-Newtonian polymers.[43] The theoretical considerations, using Maxwell fluid, lead to the conclusion that elasticity is beneficial to spinline stability. The results do not agree with the experimental determinations of fracture obtained during extension of strands of polyethylene: the samples fracture below the values of $\dot{\varepsilon}^*$ of some 40 to $50s^{-1}$ and cease to fracture again above values of $\dot{\varepsilon}^*$ of 65 to $70s^{-1}$. (Nondimensional extension rate $\dot{\varepsilon}^* = \theta\dot{\varepsilon}$ which is equivalent with the Weissenberg

number, Wi.) In the examples presented in this book, a spinline may be stable until the onset of crystallization when the Weissenberg number, calculated on the Henky's strain, reaches values close to seven, if advantage is taken of the maximum retardation time. If the retardation time corresponding to the maximum of the retardation function is taken, the corresponding values reach close to four. The beginning of change to arrheodictic behavior takes place at Weissenberg numbers 0.36 and 0.391. In this case the Weissenberg number, Wi, was calculated with the retardation times at the maximum of the spectrum and with Cauchy's strain. Clearly, it is difficult to see a relationship here.

Vinogradov[36,64] suggested that fracture, both in shear and in extension, occurs invariably between 0.1 and 0.5 MPa of true stress. The same author suggested that at the same values of stress crystallization may be starting. Analysis of the cases presented in this book as examples, as well as of many other processes, does not support this relationship to spinline instability. The build-up of recoverable work until onset of crystallization is presented in figure IV.29.

Jinan Cao[65] finds that there is a maximum in the filament velocity gradient, and flow instability starts in the area past the maximum value. In the processes presented here, there are several maxima of velocity gradient: the first one is usually close, mostly prior, to the onset of crystallization, and the others occur during crystallization and toward the end of it.

Malkin and Petrie[149], in an extensive paper, review all the efforts in solving the problem of spinline stability published through 1997. In their conclusion, the authors state that the only useful criteria are: Vinogradov's notion that failure would take place only for $Wi \geq 0.5$ (Wi = Weissenberg number), criteria resulting from the work by Reiner and Freudenthal[29] (see equations IV.33 and IV.34). Development of the ability to predict filament breaks is still found to require a considerable effort. Confusing shear and extensional properties, relaxation and retardation times, appears to be a serious flaw in the treatments published thus far – these parameters are not interchangeable.[31]

As important and as interesting as the topic is, we must still wait for a better solution to be able to take practical advantage of it. Perhaps the treatment of the fiber formation process as a case of creep experiment traveling with the velocity of polymer extrusion will allow for more definite solutions.

IV.5 Crystallization in Extensional Flow

The fact that polymers crystallize faster under influence of mechanical forces was noticed sometime in the forties.[67] The shortest crystallization half times determined dilatometrically amounted to some thirty seconds. On the other hand, total residence time of polymer in a quench zone was ranging from some fifteen down to three seconds. Despite the short residence time, it was not unusual to find that the crystallinity reached in the quench zone was equal to that found in the final fibers. A difference in the accelerating effect of forces on crystallization of different polymers was also noticed.

Probably the first attempt to study the phenomenon was published by P. Flory[151] in 1947. The work relates the temperature at which the crystallization begins to the relative extension of the molecules. In quantitative terms, the work gives the following equation:

$$\frac{h_f}{\kappa_b}\left(\frac{1}{T_m^0}-\frac{1}{T_{ci}}\right)=\frac{2\lambda l\beta N}{\pi^{1/2}}-\left(\frac{\lambda^2}{2}+\frac{1}{\lambda}\right)\frac{1}{N} \tag{IV.54}$$

where h_f is the enthalpy of fusion per chain segment, κ_b is Boltzmann's constant, T_m^0 is, as usually, the equilibrium melting/crystallization temperature, T_{ci} is initial (the highest) crystallization temperature, N is the number of segments per polymer chain, l stands for the length of a segment, $\beta=(3/1Nl^2)^{1/2}$, λ is the extension of polymer chain (equivalent to draw ratio as $\lambda=1$ means no extension).

Equation IV.54 is difficult to confront with experiments since the quantities obtainable experimentally are not easily translated into the parameters of the equation.

Van der Vegt and Smit[68] seem to have originated experimental studies of the influence of shear on the initiation of crystallization. The authors melted polypropylene in a capillary rheometer, cooled it somewhat and extruded at increasing shear stress. Initially, the polymers behaved normally, but after a certain value of stress had been exceeded, viscosity started to increase, sometimes rapidly. The increase of viscosity was attributed to the onset of crystallization. The shear stress and shear rate at which the crystallization began depended on the temperature of the experiment. At $160°C$, crystallization started at some 1.2 s^{-1} shear rate and about 45.7 kPa, while at $180°C$ the respective values were some 38 s^{-1} and 113.6 kPa.

In a follow-up of the van der Vegt-Smit experiments, it has been determined[134] from synchrotron X-ray diffraction that during extrusion, a "mobile mesophase" of hexagonal organization may form in capillaries, which under appropriate conditions, in terms of shear rate and/or temperature, may crystallize to freeze the capillary. Formation of such a mesophase does not take place in the entry to a capillary where the elongational flow predominates.

Similar semiquantitative experiments were performed during fiber formation experiments.[69] A flat plate X-ray camera had been installed on a fiber formation machine on which also temperature was measured with an infrared thermometer. It had been found, depending on the amount of draw, that the first sign of polypropylene crystallization could be noticed at filament temperature ranging from $160 to 180°C$. In polypropylene of molecular mass amounting to approximately 450000, thirty five per cent of crystallinity was reached within 102 ms.

The X-ray technique has been found very useful for the investigation of the onset of crystallization, and particularly for the development of orientation and other structural features.[69] It has been found essentially inapplicable for determination of the crystallization kinetics – an immensely important aspect of the entire process of fiber formation. Another technique for the purpose has been developed, which may be called determination of the *crystallization history*, or

CH for short.[70] The principle of the method is based on the relationship existing between the crystallization temperature and the melting point. (See also section II.2.b.) The principle of the method is simple, the instrument needed is the rather common differential scanning calorimeter (DSC), possibly of fast response. High quality, high precision experimental work is needed, as well as rather extensive calculations. The last problem is easily solved by computers, once the proper programs are available.

The following sequence of work is involved: initially one needs to perform as large as practical number of isothermal crystallizations, followed by immediate melting to determine the relationship between the crystallization temperature and the melting point. The equilibrium melting point is obtained at the same time. High accuracy data are needed, as the extrapolation to the equilibrium melting point is usually far reaching. As high as possible crystallization temperature is advisable, though caution is needed to avoid degradation of the polymer during a prolonged time at an elevated temperature. A simple graph, like that in figure IV.27, may be obtained together with an equation:

$$T_{melt} = a + bT_{crist} \tag{IV.55}$$

where

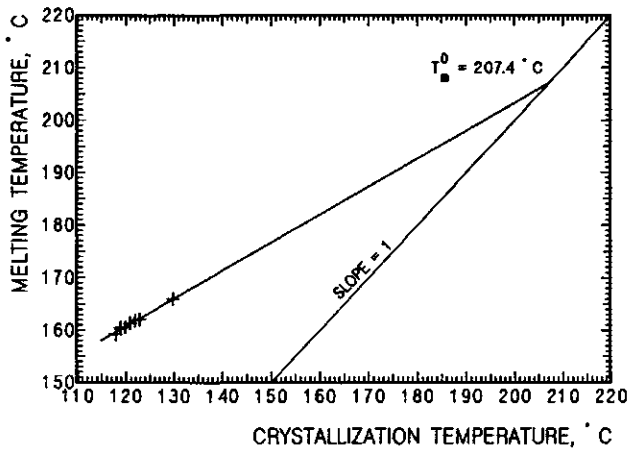

Figure IV.27: *The relationship between crystallization temperatures and melting points in a propylene polymer.*

$$T_m^0 = \frac{a}{1-b} \tag{IV.56}$$

In many instrumental analytical techniques, one has to deal with a problem generally referred to as *instrumental line broadening*. This means that what theoretically ought to be presented as a *mathematical line* in reality appears as a peak of some finite breadth. The most common reason for line broadening is the finite response time of the instrument and a finite rate of the investigated phenomenon. For example, if we melt a low molecular weight crystal in a DSC apparatus at

a given heating rate, the specimen requires some finite time to melt completely. Nevertheless, in that increment of time the instrument temperature climbs higher, and as a result we obtain a peak. The effect of process rate and of instrument response time superimpose to widen the broadening. In some processes, the polymer crystallization phenomena included, we have to deal with process/structure imperfections. A polymer chain with a slightly crippled structure, in comparison to its perfect half-brother, or just some more dense chain entanglements, may require a slightly larger degree of undercooling to crystallize and will also melt at lower temperature. This leads to an additional reason for peak broadening which is structure related and which may be specimen specific.

Correction for peak broadening was applied first to X-ray diffractograms in the early forties. The technique used for the purpose was deconvolution. If we denote the original function as $f(t)$ and its Fourier transform[71] as $\Im$, then

$$\Im = \int_{-\infty}^{\infty} f(t) \exp(-2\pi\nu it) dt \tag{IV.57}$$

If we then denote $f(t)$ the true melting function, $f_b(t)$ the peak we obtain from the instrument, and $f_e(t)$ the experimental melting function, and $\Im$, $\Im_b$, $\Im_e$ the respective Fourier transforms, then we may write a convolution equation:

$$\Im * \Im_b = \Im_e \tag{IV.58}$$

and further

$$\Im = \Im_e / \Im_b \tag{IV.59}$$

In practice, as a Fourier transform of a function we take the following representation:[71]

$$f(t) = \frac{A_0}{2} + \sum_{j=1}^{n} \left(A_j \cos j\frac{2\pi t}{T} + B_j \sin j\frac{2\pi t}{T} \right) \tag{IV.60}$$

and the coefficients of the transformed function are:

$$A_j = \frac{2}{m} \sum_{k=0}^{m-1} y_k \cos j\frac{2\pi k}{k} \tag{IV.60 a}$$

$$B_j = \frac{2}{m} \sum_{k=0}^{m-1} y_k \sin j\frac{2\pi k}{k} \tag{IV.60 b}$$

where m is the number of equally spaced discrete points representing the function, n is number of harmonic equations, preferably $n \leq m/2$.

The coefficients of the deconvoluted function are obtained according to the division of complex numbers:

$$A = \frac{(A_e A_b + B_e B_b)}{(A_b^2 + B_b^2)} \tag{IV.61}$$

$$A = \frac{(A_b B_e - A_e B_b)}{(A_b^2 + B_b^2)} \qquad (IV.61\,a)$$

It is common that deconvoluted functions may display "rumblings", that is, a series of maxima and minima located at the left and right peripheries of the investigated peak. The only remedy available to limit such "rumblings" to an acceptably low level, or to a range sufficiently distant to be unimportant, is to limit the number of the harmonic equations used to calculate the final deconvoluted function. Generally, good operator's judgment is necessary in such cases.

The question of the proper deconvoluting function is not completely closed. This author finds that the best results were obtained with functions generated from controlled crystallization at low rate of cooling (nonisothermal) and melting curve from the same controlled crystallization run. The critically important point is that the polymer must be the same as the sample investigated. The same is true of the determination of the $T_m = f(T_c)$ relationship. It must be the same polymer batch. Even small differences between different samples of polymer are sufficient to wreck the accuracy, or even the entire sense, of the determination. For example, if fibers are investigated - fibers are to be used, not the pellets or melt prior to the extrusion. One needs to observe some differences in long periodicity due to molecular mass, polymer perfection, etc.[129]

One may consider, and some special cases may require, the use of other functions for deconvolution. A combination of functions is possible. In the last case, e.g. two isothermal functions, a low and a high temperature, may be combined. The interpolated deconvolution function is simply a sum of the proper fractions, φ, of the Fourier coefficients:

$$A_{ja} = \varphi A_{j1} + (1 - \varphi) A_{j2} \qquad (IV.62)$$

$$B_{ja} = \varphi B_{j1} + (1 - \varphi) B_{j2} \qquad (IV.62\,a)$$

One must stress that there is some controversy regarding the crystallization - melting temperature relationship. It is true that at low crystallization temperature, the points do not follow a straight line. If the lowest range of temperature is of interest, a caution may be advisable. Some investigators suspect that the $T_m = f(T_c)$ function is not represented by an exactly straight line, but it curves somewhat upwards. However, if the procedures just described are followed exactly, some of the potential errors may cancel themselves out. On the other hand, for the time being there is no other method which would permit analysis of the extremely rapid process of crystallization. As will be seen below, the accuracy of the obtainable results is sufficiently high to satisfy even very demanding investigators.

The relationship between crystallization and melting temperatures may be affected by cold drawing (plastic deformation). Experience, in agreement with the theory, shows that small extent drawing may be well neglected, as the discrepancies would not exceed the experiment's error. More extensively drawn samples may present problems. The best choice, naturally, is utilization of specimens prior to any drawing operation.

The sequence of all the experimental DSC runs, aside from the determination of the crystallization - melting temperature relationship, is as follows:

- Melting of the polymer (fiber) specimen investigated (preferably at 10 to 20 $°K/min$, depending on the response time of the instrument, up to a temperature of 20 to 40 $°K$ above the equilibrium melting point and holding for some ten minutes to assure full melting. Higher molecular mass polymers may require more severe conditions.

- Crystallization at a low cooling rate (2 to max. 5 $°K/min$), depending on the crystallization propensity of the investigated polymer. To shorten the run time, the initial forty to seventy degrees may be dropped at as fast a rate as the instrument may safely handle, without losing full temperature - time control.

- Upon completion of the crystallization run, immediate melting of the specimen at the same heating rate as during the first melting operation.

Naturally, all the baselines should be calculated to respect the baseline change due to the change of the heat capacity during the transition.[79]

The procedure described above yields three scans. From the third scan (melting curve) and the second scan (controlled crystallization curve), one obtains the deconvoluting function which is used to deconvolute the first melting curve (the first scan).

A word of caution is needed. When investigating polymers which crystallized under the influence of forces, one may find some unexpected shapes of the crystallization curves, which will become evident in figures IV.29 and IV.30, where crystallization history curves are reproduced.

Since the initial work of Flory[151], there have been several attempts to solve theoretically the problem of crystallization under influence of forces.[72–78] Unfortunately, none of the suggested solutions could accommodate the determinations obtained from a substantial number of experimental data. Intuitively, and in an agreement with the sense of the Flory's stipulations, the most promising appeared to be the suggestion by Cahn[72] and Hilliard[73] that the stored work input is responsible for the accelerating effect. Confrontation of this idea with the experimental data shows that the stipulated relationship indeed has merit.

As it was shown in section IV.4.c, from the retardation functions one may calculate the work input in creep. The work input, both the stored and the dissipated work, initially increases gently, then accelerates strongly at some point, very much in line with the changes of velocity to which it is connected. Figure IV.28 illustrates the stored and the dissipated work during fiber formation plotted against time. The results beyond the onset of crystallization are not necessarily "legitimate" due to the presence of crystalline phase in the fluid.

The word *initiation of crystallization*, similarly as the *end of crystallization* may sound somewhat nebulous as the crystallization rate function is vanishing to zero at both ends. For the sake of communication in real life, in this context we

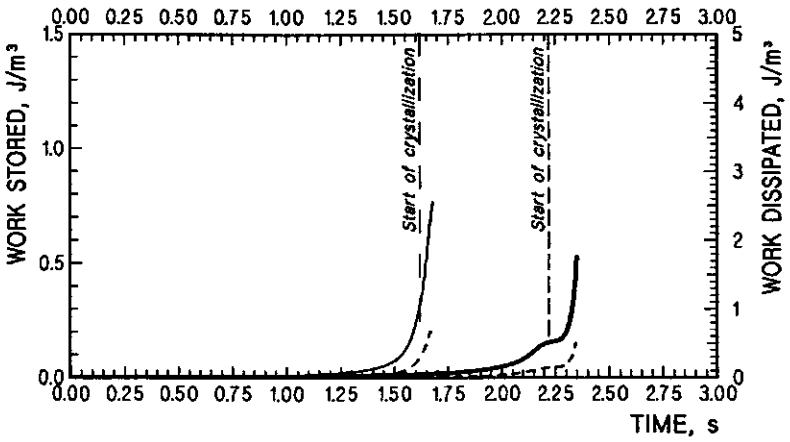

Figure IV.28: *Stored and dissipated (dashed lines) work in a process of fiber formation from polypropylene. Data to the beginning of crystallization versus time from die swell. Heavy lines : case from figure IV.23. Finer lines: case from figure IV.24.*

define the term as the point where the value of the rate function becomes larger that 0.001, or smaller than 0.001 for the beginning and the end of the process, respectively.

To quantify the crystallization processes, the Fisher-Turnbull, or otherwise called, Hoffman-Lauritzen, equation (equation II.20), as imperfect as it is, is used. An accelerating coefficient for the nucleation term was calculated using the equation coefficients as found from the least square fit of the quiescent, or "natural crystallization", curve obtained in a differential scanning calorimeter and a modified equation I.20 in the form given here as equation IV.63. An accelerating factor F_w for the heat of fusion was calculated to obtain the agreement with the experimental strain accelerated curves. Figures IV.29 through IV.32 show the results of such operations for two cases.

$$I^* = K_0 T \exp\left\{-\frac{32\ K_n (T_m^0)^2}{[\ \Delta H_f F_w T (T_m^0 - T)]^2}\right\} \exp\left(-\frac{K_f E_a}{RT}\right) \qquad \text{(IV.63)}$$

The factor correcting for the polymer flow, F_w, does not add to the heat of fusion, as expected by Hilliard[73], rather it multiplies it. The back calculated curves with an application of the experimentally, so to speak, determined factor superimpose exactly with the curve as obtained from the crystallization history determination. The accelerating factor at the point where crystallization starts may be presented according to the following relationship:

$$T_{ci} \times \left(\frac{T_m^0 - T_{ci}}{T_m^0}\right) = T_{ci}^* \times \left(\frac{T_m^0 - T_{ci}^*}{T_m^0}\right) \times \exp(W_{s,icr}) \qquad \text{(IV.64)}$$

In equation IV.64, $W_{s,ci}$ stands for the work stored up to the point of initiation of the accelerated crystallization, T_{ci} is the temperature at which the quiescent

crystallization is initiated, and T_{ci}^{*} is the initial temperature of crystallization under the influence of stored work. Other designations are as usual. When considering crystallization beyond the point of initiation, it is necessary to correct the stored work for the "freezing" of the nuclei or strains by the developing crystallinity. Finally, it leads to the following form for the correcting factor

$$F_w = \exp(W_s)(1-\alpha) \tag{IV.65}$$

The equations IV.64 and IV.65 hold well only for the point of crystallization initiation. The segment of the curve describing crystal growth does not describe the experimentally obtained crystallization curve. If the amount of crystallinity developed up to a given time, α, is omitted in equation IV.65 then the correcting factor is strongly excessive and displaying some pulses coinciding with the beginnings of each crystallization peak. Introduction of the correction for freezing the work input by crystallization deepens the pulses. If a correcting factor calculated according to equations IV.64 and IV.65 is applied to the whole temperature range of a crystallization, somewhat surprising results are obtained. Very sharp, extremely large peaks are obtained at the beginning of each experimental peak. Equation IV.63, as originally developed by Fisher and Turnbull[143], and in all its different later versions, essentially describes only nucleation. That the nucleation is the slowest link of the crystal growth, and as such determines the overall rate of the crystal growth is taken as an axiom. Here we may see that the rate of nucleation is extremely fast, almost in explosive bursts reaching values of 10^{30} or higher, reaching numbers which are substantially higher than the physical possibilities. However, the growth of the crystals follows substantially slower. Figures IV.29, and IV.30 represent four different cases evaluated as just described. The correlation is excellent with the point of initiation of crystallization. The rest of the process remains largely unknown. Additional description of the processes given in figures IV.29 and IV.30 is given in Table IV.2.

Table IV.2.
Conditions of the processes presented in figures 4,29 and 4,30.

Figure	η_0 $Pa \cdot s$	σ_0 kPa	W_{ci} J/cm^3	$T_m^0 - T_{ci}$ $^\circ K$	t_{cr} ms
IV.29 top	193.6	16.973	0.2722	46.41	125,8
4,29 bottom	142.6	18.728	0.2855	48.81	101,9
IV.30 top	167.9	6.475	0.1485	62.79	74,1
IV.30 bottom	161.6	9.472	0.1888	56.59	61.6

The first important conclusion to be reached is that the rate of nucleation may be substantially higher than the rate of crystal growth. Similar conclusions may be drawn from fitting the experimental unaccelerated crystallization curves into the Hoffman-Lauritzen equation. In some cases, the experimental curve lags somewhat behind the calculated (figure II.9), but there the small differences may be often attributed to an experimental error, or to the imperfection of the equation. There

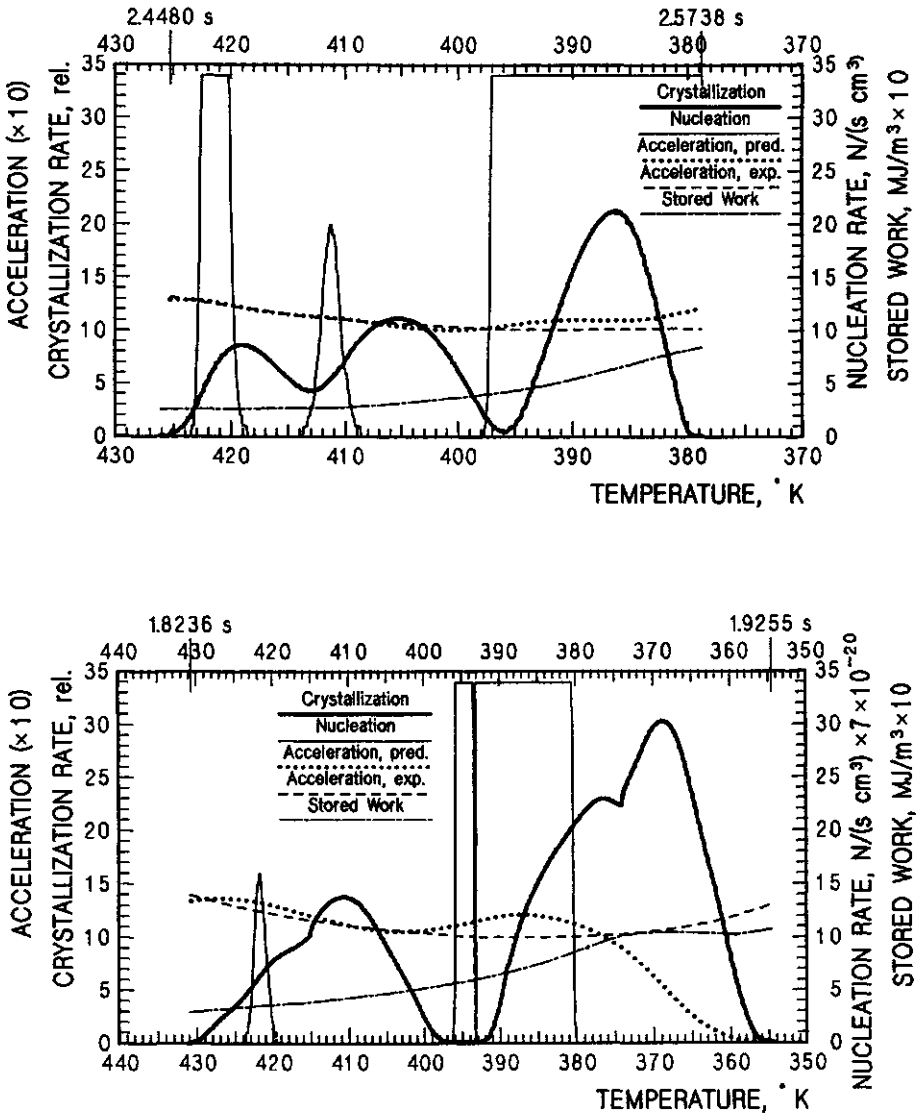

Figure IV.29: *Crystallization rates (heavy lines) and nucleation rate (finer line) during fiber formation versus temperature. Dashed line: accelerating factor from comparison with free crystallization curves. Dotted line: factor from equation IV.65. Dash-dotted line: stored work. Details in Table IV.2.*

is, however, no workable theory describing the rate of crystal growth, leave alone growth at strain accelerated conditions.

There is a number of unanswered observations concerning the interrelations

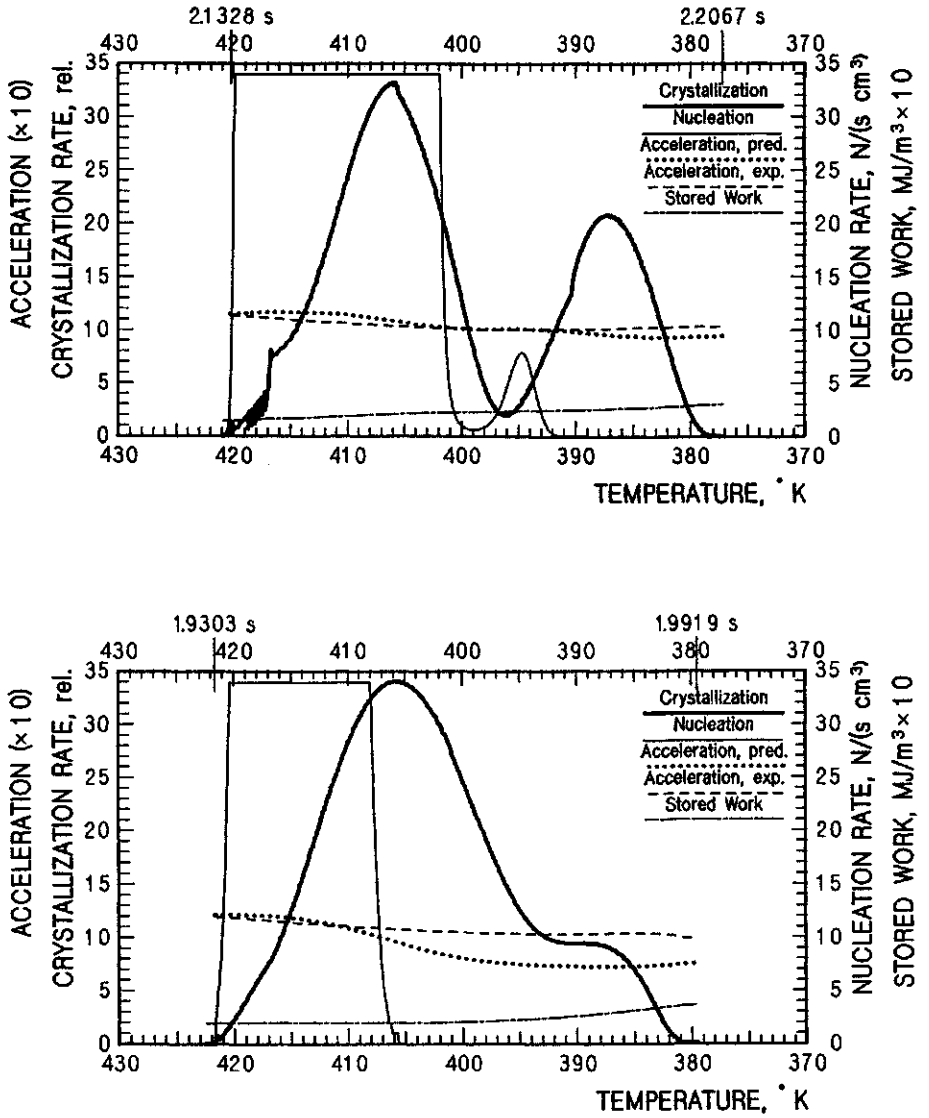

Figure IV.30: *Crystallization rates (heavy lines) and nucleation rate (finer line) during fiber formation versus temperature. Dashed line: accelerating factor from comparison with free crystallization curves. Dotted line: factor from equation IV.65. Dash-dotted line: stored work. Details in Table IV.2.*

between rheology and crystallization, they may be summarized as follows:

- One may notice that nucleation is invariably connected with a decrease of extension rate, and that this decrease is in some proportion to the size of

the nucleation peak.

- A large number of nuclei influences the rate of work storage, which seems to be connected to the point above.

- It may be admitted that the "excessive" nucleation in reality represents a nematic or smectic morphology, as described for the case of poly(ethylene terephthalate).[154] Nevertheless, direct comparison of crystallization of polypropylene and of PET calls for caution. Crystallization of PET is approached from temperatures lower than the glass transition, while crystallization of polypropylene is approached from the temperature of the melt. Polarity of PET may also be not without significance.

- Apparently great numbers of the formed nuclei must be either destroyed by the flow or "wasted" in some other way.

- Outside of the nucleation peaks, during crystal growth, the extension rate generally increases. One may suggest that the extensive nucleation forms a "homogeneous network", while crystal growth forms crystalline mats consisting of mosaic blocks which leads to some inhomogeneity. Points of stress concentration may lead to a partial break of the structure and to increase in strain. Similar changes in morphology may be responsible for the arrheodictic portion of the creep behavior.

- Interpretation of growth is only speculative. The stored work increases, in some cases very sharply, but crystal growth is by far not commensurate with it. One may even suppose that an increase of energy beyond some point slows the crystal growth. Analysis of the data of Table IV.2 indicates that total time of crystallization, t_{cr}, is shorter for those processes which employ lower initial stress, σ_0. At the same time one may notice, however, that the lower initial stress requires larger undercooling, $T_m^0 - T_{ci}$.

- The full crystallization times of the energy accelerated processes are shortened 550 times to well over one thousand times. From the cases presented here one may infer that the higher acceleration takes place when the stored work does not increase too rapidly.

- Very often the accelerated crystallization process proceeds down to the same low temperature as unaccelerated process does, or even markedly lower.

The development of a quantitative description of the growth kinetics, as difficult as it may be, is indispensable for any further progress in the field. It appears that for progress in this area, consideration of chain entanglements and their influence on the molecule mobility, transport, and extension of molecule segments might be essential.[135] Perhaps a flow equation would also give better agreement between the Fisher-Turnbull equation and quiescent experiments.

There is one more observation of utmost importance, which appears to agree well with the above given findings: a fast crystallization process results in larger

crystallites, a slow process gives smaller crystallites. It is exactly opposite to the cases of crystallization of low molecular mass compounds. One may suppose that the stored work factor which accelerates nucleation represents relatively permanent changes in the morphology of molecules. On the other hand, more intense flow of the molecules past one another disturbs the growth process. This finding also explains some of the old observations of various processes and relationships between processing conditions and fiber properties.

It is necessary to stress the good agreement between the results of such different analytical techniques utilizing many different instruments, both on various formation machines and in a characterization laboratory. All these results underwent extensive mathematical treatment and all agree within one or two per cent, or one or two degrees in temperature deviation. This agreement serves as an indication of a great coherence, and thereby a great reliability, of the interpretive system. As will be seen in the following chapters, this coherence extends still much further than so far described.

One may point to the disturbances in the beginning of the crystallization curve in figure IV.30 top. They might be taken as an artifact of determination of the crystallization history. In fact they are due to slight fluctuations in the stored work, which is only faintly visible in the figure due to large scaling factor. At any rate, even the disturbance has its justification.

A recently published paper[153] describes an investigation of the crystallization of amorphous poly(ethylene terephthatale) under influence of strain. The process was monitored by synchrotron X - ray analysis. Contrary to many other papers of such type, the experiments were well designed, without "mixed up" variables. The work confirms almost all the findings reported above. The strain induced process requires a critical degree of chain segment orientation which is dependent on temperature and draw ratio. The draw ratio represents a substitute for the stored energy. In the experiments reported[153] the process of crystal growth below $125°C$ started invariably after cessation of strain and ran to completion according to the first order transformation within one second. The rate of crystallization appears to be insensitive to temperature, indicating activation energy of $1kcal/(mole \times° K)$, or less, which is in a strong contrast to some 40 $kcal/(mole \times °K)$ for quiescent crystallization process. Above $125°C$ the process of relaxation is faster and the "oriented non-crystalline segments" formed during straining below $125°C$ are not formed above the critical temperature. One may inject here that polypropylene usually has higher molecular mass and much higher melt elasticity, consequently the degree of acceleration of nucleation ought to be correspondingly higher. Also, the critical temperature for no- nucleation may be expected to vary with molecular mass. Nonetheless, direct comparison of crystallization of polypropylene and of PET calls for a caution. Crystallization of PET is approached from temperatures lower than glass transition, while crystallization of polypropylene is approached from the temperature of the melt. Contrary to polypropylene, PET is polar, and this is not without a significance. The authors[153] also anticipate the possibility that a network of nuclei, or a mesophase, hinder the molecule, or segment, mobility

thereby restricting the crystallization.

One may conclude, as far as the smaller number of background data (rheology, crystallization history) permits, that the published work[153] presents a far reaching confirmation of the investigations of polypropylene crystallization described above.

In summary, one may conclude that the theoretical solution of crystallization process is far from satisfactory. The available equations may be used as a working tool but only as far as the initiation of crystallization is concerned. The nucleation segment of the equation may be close to being correct, but the rest of the factors influencing kinetics still need to be defined.

IV.6 Cold Drawing

In 1932 W. H. Carothers and J. W. Hill[80] have described a "peculiar" property of *as spun* polyester fibers. Namely, the fibers could be drawn at temperature ranging from room temperature to somewhat elevated temperatures, but less than the lowest melting point, and when the fiber was subjected to a sufficiently high force its diameter decreased abruptly forming a characteristic "neck", resembling

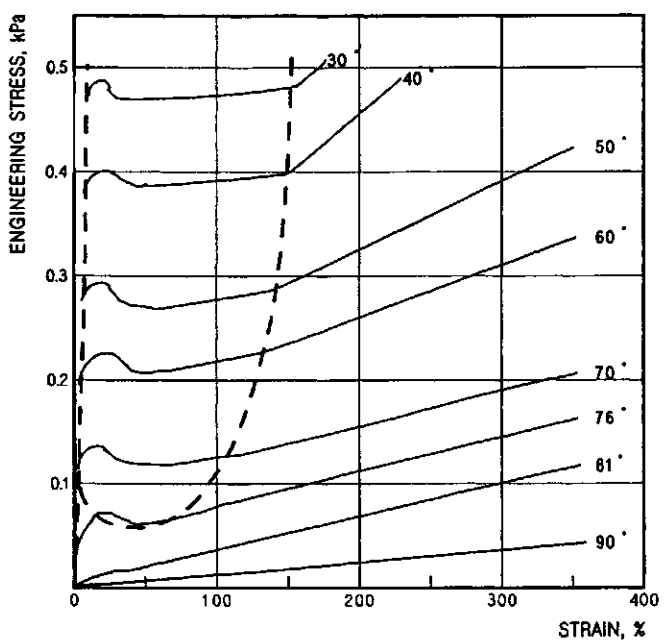

Figure IV.31: *Initial (engineering) stress - strain curves for cold drawing of chlorinated poly(vinyl chloride) at various temperatures. The dashed curve encompasses onset of the yield point and natural draw ratio until end of necking. Data from F. H. Müller*[81].

a bottle neck. A drawn specimen had a distinct boundary between the drawn, transparent, and undrawn, opaque sections of appropriately different diameters. This operation leads to fibers of uniform diameter possessing a structure orienta-

tion.

The diameter attenuation in cold drawing is not limited to the neck area. Only the initial portion of the total cold drawing extension takes place in the neck, the reminder takes place past the necking zone. It is generally assumed that the cold drawing temperature spans from some distance below the glass transition point up to the "lowest detectable" melting point. In reality the temperature range, as well as some other parameters of cold drawing depend very strongly on the amount of crystallinity and morphology of the *as spun* fibers and on the conditions of the drawing process. Stress strain curves of a cold drawing process for different temperatures are shown in figure IV.31 The thick dashed line encompasses the necking area, from the onset of yield to the *natural draw ratio.*

A few words need to be said about the semantics. The term *cold drawing* has been coined by the fathers of synthetic fibers and it may be a matter of needed courtesy to keep it, despite the fact that the drawing is not necessarily *cold.* Other terms may be found in the literature of the subject: *drawing with the neck formation* or simply *neck drawing*, or a term derived from structural and property considerations *plastic deformation.* There may be some confusion created by the fact that in some circles, particularly those of the fiber industry, the term cold drawing has been reserved to mean the drawing at a temperature below the glass transition for the polymer in question.

IV.6.a Mechanism of Drawing

The theoretical explanation of the discontinuous nature of cold drawing was the subject of numerous publications[82,94] over many years. All of these works were based on the same principles of so called *thin filament equations*, which represent a simplification of the theories of hydrodynamics and rheology. Also, it was believed that the necessary condition for a necking to take place is that the relation between strain and force must have an "S" shape, with a distinct minimum before the force goes up again, beyond the first maximum (figure IV.33 A).

This approach has been subjected to a convincing critique by S. Kase and M. Chang[95], who started from the same assumptions as in the previous work. Consideration of inertia in their solution led to the realization that the obtained equations are equivalent with the equations used in the area of *dynamic plasticity.* The basic equation in nondimensional form is:

$$\frac{\partial^2 \eta(X)}{\partial \lambda^2} = C_1 \frac{\partial^2 X}{\partial \tau^2} \tag{IV.66}$$

Here η is nondimensional tensile force, X is elongational deformation, λ is one dimensional space coordinate (Eulerian), and τ it time. Upon substitution of Hookean elasticity,

$$\eta(X) = X - 1 \tag{IV.67}$$

For $\eta(X)$, the authors[95] obtained the wave equation:

$$\frac{\partial^2 X}{\partial \lambda^2} = C_1 \frac{\partial^2 X}{\partial \tau^2} \tag{IV.68}$$

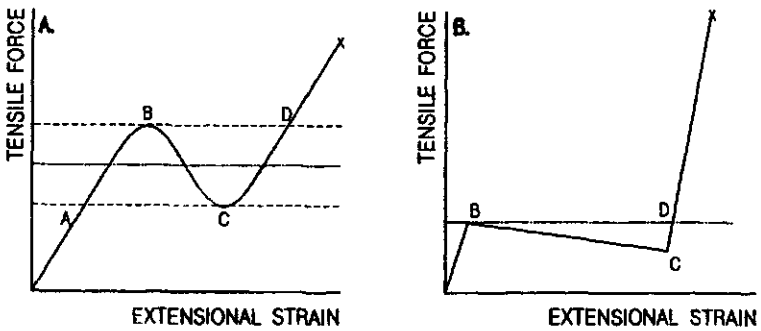

Figure IV.32: *Schematic representation of the type of relationship between tensile force and extensional strain necessary for a neck formation. A. for "rheological" theories*[82,94], *B. for the solution by S. Kase and M. Chang.*[95]

C_1 stands here for the inertia coefficient. Equation IV.68 is applicable to very fast plastic deformation problems, for example, determination of damage done by bullets. In the dynamic plasticity, the equation is used in somewhat different form:

$$V^2 \frac{\partial^2 u}{\partial \lambda^2} = \frac{\partial^2 u}{\partial \tau^2} \tag{IV.69}$$

$$V^2 = \frac{1}{\rho} \frac{d\eta(X)}{dX} \tag{IV.69 a}$$

where

$$X = \frac{\partial u}{\partial \lambda} \tag{IV.70}$$

where λ is one-dimensional Langrangean space coordinate, τ is time, u is displacement, ρ is material density, and η represents true compressive stress, X is infinitesimal deformation, V is wave velocity dependent on X. Equation IV.68 becomes equivalent to equations IV.69 - IV.70 when ρ in equation IV.69a is replaced with C_1. Then equation IV.69 represents the wave propagation at a velocity dependent on X:

$$V = \sqrt{\frac{1}{C_1} \frac{d\eta(X)}{dX}} \tag{IV.71}$$

At this point, Kase and Chang[95] draw the analogy to a very strong impact imposed on an aluminum rod, which produces two waves (see figure IV.33). The elastic wave A is propagating with the speed of sound in the material. The plastic wave B is moving with velocity V represented by equation IV.69, much slower than velocity of sound. In the form of wave A, the material is free of stress, between the waves A and B it is in an elastic compression, and it is in a plastic compression behind the yield form represented by wave B.

Kase and Chang[95] solved equation IV.69 numerically, the solution method is described in detail in the original paper. When for the solution was used a

Figure IV.33: *Elastic wave A and plastic wave B propagating in an aluminum rod. Reproduced after Kase and Chang.*[95]

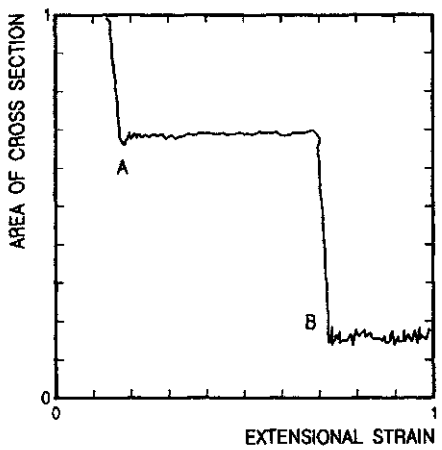

Figure IV.34: *Relationship between the extensional strain and the cross sectional area of a filament (both values nondimensional) resulting from equation IV.69 when constitutive function of figure IV.32B was used, including plasticity hysteresis. From Kase and Chang.*[95]

constitutive curve, like that in figure IV.33A the resulting description of necking represented a smoothly wavy curve. When a constitutive equation of the form given in figure IV.32 B was used, a representation of an abrupt, step change of the cross section area resulted. Such a curve is reproduced in figure IV.34 The calculations were done for the case of poly(ethylene terephthalate) with the sound velocity in the polymer of $v = \sqrt{E/\rho} = 1350\ m/s$.

The smoothness of the numerical calculation was greatly improved by the introduction of the plasticity hysteresis curve into the $\eta_{\parallel}(X)$ function of figure IV.32 Without the consideration of the plasticity hysteresis, the obtained curves showed excessive noise.

The process of cold drawing still cannot be considered solved. Approximately at the same time when Kase and Chang published their paper, A. I. Leonov[96] published a derivation of the S-shape constitutive curve as resulting from surface tension. For now, there appears to be slightly too many theories that make sense and still lack of a definite one. Rather intensive work on the subject is being continued, new papers bring additional contributions, however, a definite solution

appears to be still a number of years away. Oleinik and co-workers[97,98] find that the initiation of drawing yield is governed by several different mechanisms, which may well explain the difficulties in finding a general solution. Also, the majority of the work published, understandably, is concerned with drawing at relatively low, or very low, velocities, which are closer to testing conditions than to industrial cold drawing processes.

Among the more interesting observations one is compelled to quote those by R. N. Howard[99,100], which offer a relatively simple solution. According to this proposal, cold drawing, particularly the post yield part of it may be described by a combination of the Gauss equation

$$\sigma_{true} = Y + G_p\left(\lambda^2 - \frac{1}{\lambda}\right) \tag{IV.72}$$

and the Eyring equation

$$\frac{1}{\lambda}\cdot\frac{d\lambda}{dt} \propto \exp\left[\left(\frac{E_0}{kT}\right) \times \sinh\left(\frac{\alpha\sigma}{kT}\right)\right] \tag{IV.73}$$

which has been simplified for isothermal cases to

$$\frac{1}{\lambda}\cdot\frac{d\lambda}{dt} = A\exp(B\sigma) \tag{IV.73 a}$$

where σ stands for true stress, Y is yield stress (extrapolated), G_p is the strain hardening modulus, $\lambda = l/l_0$ is extension ratio, α is a constant with dimension of volume, A and B are constants. The resulting new Gauss-Eyring equation is

$$\frac{d}{d\lambda}\left[\ln\left(\frac{1}{\lambda}\times\frac{d\lambda}{dt}\right)\right] = B\left[\sigma_0 - G_p\left(2\lambda + \frac{1}{\lambda^2}\right)\right] = I_n \tag{IV.74}$$

Here σ_0 is initial, "engineering" stress, and I_n has been named the *localization index*, as it determines if the rate of strain in a segment increases or decreases with the increasing strain under applied load or stress. At the beginning of the deformation at λ close to unity, equation IV.74 may be approximated by

$$I_{n(\lambda\approx 1)} = B(\sigma_0 - 3G_p) \tag{IV.75}$$

The constant B under isothermal conditions is equivalent to α, and B together with G_p and with the applied stress, σ_0, determine the mode of deformation. Also, at the beginning of a constant load or constant rate of extension, σ_0 may be identified with the yield stress. This is helpful in determining the ratio of Y/G_p. Necking has been determined by Considere[101] and Vincent[102] to occur when $Y/G_p = 3$.

The localization index initially rises, at the yield point it passes through zero and then turns negative above the critical value of λ, designated as λ_c. Such a course of events is characteristic for a stable necking. On the other hand, with the decreasing strain rate the yield strain increases.[110]

The rate of strain in the neck rises initially and later starts to fall. The point where the rate of strain reaches the value it has in the undeformed material determines the *natural draw ratio*, λ_D. This point coincides with the point where the engineering stress reaches again the value it has at the yield point. The value of λ_c may be calculated according to the equation:

$$Y/G_p = 2\lambda + 1/\lambda^2 \tag{IV.76}$$

The strain hardening modulus, G_p, depends on the molecular mass and it is independent on crystallinity. Several authors[103,107] have found that the materials with a higher molecular mass show a lower natural draw ratio and the molecular mass increases the strain hardening modulus.[109,100]

An approach similar to that by R. N. Howard has been taken later by other authors[132,133] with basically similar conclusions.

An interesting interrelation between the draw ratio, λ, and temperature has been reported by Butler *et al.*[111] The authors distinguish four drawing areas:

1. At very small final strains, smaller than the yield point, the drawing tension and the location of the draw zone fluctuate, a nonuniform cross section fiber is obtained.

2. At somewhat higher strains, one reaches a point "where the entire length of the fiber undergoes a drawing". If the final strain in this area is insufficiently high, the fiber may still show some diameter nonuniformities. The tension fluctuations are here less than in zone 1. The highest strain for this area produces the most uniform fibers, the necking is well defined, the tension fluctuations are at a minimum.

3. As the strain is further increased, the extension takes place in the neck and beyond, therefore, a second stage of drawing is formed, (*post yield draw*). A wide range of draw ratios is possible in this area.

4. With further increase of the draw ratio, the necking area becomes unstable. The obtained fibers may still be uniform and of a considerable strength. The drawing conditions here are poorly defined and the process is not under full control, as is the reproducibility.

The delineation of the different drawing zones depends on the temperature, at lower temperatures, the transition between zones two and three shift toward higher draw ratios. In the view of the authors,[111] if the draw ratio enters in the third area, the process should be conducted in two steps for optimum effects in the drawing operation: one strictly neck drawing to the natural draw ratio, and in a separate step the post yield drawing with a separate temperature and tension control.

The above quoted continuum theories represent a fair approximation of the described process. Whether substantial further progress will be made on this path may be debatable. Kasai and Kakudo[112] conducted a very detailed X-ray study of

the neck zone. A three millimeter thick rod was drawn to a ratio of 7.5. The neck area has been sectioned to 0.3 mm thick slices, and the so obtained specimens were investigated small segment by a small segment along the material stream lines with micro X-ray equipment. Naturally, only the fate of the crystalline portion of the material was studied.

The process, in the investigated specimen started with aligning the a-crystallographic axis nearly perpendicularly to the stream lines, and subsequently the c-crystallographic axis started to align along the stream lines. Similar conclusions had been reached earlier by Aggarval and co - workers[113] Initially, along the center line, the crystallite size remains unchanged, while in the side stream lines, the crystallite size increases. The degree of the increase becomes gradually larger when moving from the center to the specimen surface. In the later stages of the process, the crystallite size decreases, and when the orientation of the c- axis is almost exactly parallel, the crystallite size is about half of its original size. Similar work was performed later by Kuksyenko *et al.*[114] and the authors essentially reiterated the conclusions drawn by Kasai and Kakudo.

Whatever conclusions have been reached[113,114], they relate to the highly crystalline materials drawn under one set of conditions. The process for low crystalline materials is thus far not exactly known. Nonetheless, based on the above quoted studies one may doubt whether continuum theories may be the appropriate tool to describe the process. The structural aspects of cold drawing will be discussed in more detail in the chapter on fiber structure.

From the structural studies, it results that the drawing process affects primarily the noncrystalline portion of the polymer. According the the classical rubber elasticity theory[115], it is known that the drawing process decreases entropy; it is a decrease of the configurational entropy associated with the molecule orientation.

$$-\Delta S_c = \left(\frac{R}{2\alpha}\right)\left[\lambda^2 + \left(\frac{2}{\lambda}\right) - 3\right] \tag{IV.77}$$

where α is the number of monomer units between entanglements, and λ is the draw ratio.

One of the effects of the entropy change is an increase of melting point due to drawing.[116 *and ref.*] Equation IV.75 has been combined[116] with the equations for the melting point of folded chain crystals to yield

$$\frac{1}{T_m} - \frac{1}{T_m^0} = \left(\frac{RT_m^0}{2x\alpha T_m \Delta H}\right)\left[\lambda^2 + \left(\frac{2}{\lambda}\right) - -3\right] \tag{IV.78}$$

where x is the degree of polymerization, and the remaining symbols have their traditional meaning. For polyethylene, the slope of the reciprocal melting point *versus* the drawing term, $\lambda^2 + 2/\lambda - 3$, has been found to be $4.9 \times 10^{-8}\,\mathrm{deg}\,K^{-1}$. This influence is so small that for the majority of the commercially drawn fibers it may easily be neglected.

Very recent studies[144 *& ref.*] relate the drawability, particularly the more extensive draw ratios, and the drawing performance to the α_c relaxation corresponding

to the Peterlin's T_α temperature (see section II.2.b). The α_c relaxation indicates the onset of translational motion of the polymer chains along the *c*- crystalline axis. It is quite obvious that it must strongly depend on the structure of the polymer chain. Large side groups are able to suppress the translational motions down to zero, which results in so called *crystal - fixed polymers*[144], or otherwise *nonductile crystals.* Strong hydrogen bonds have a similar effect, like in nylons. High molecular mass polymers theoretically permit more extensive drawing. Chain entanglements also suppress the α_c transition. Since long chains are more apt to high entanglements, the high molecular mass polymers not always may be drawn more intensively. Increase of temperature causes increase of the crystalline α_c relaxation. Hu and Schmidt - Rohr[144] stipulate that drawing involving chain translations is possible when the rate of α_c transition is larger than $10^3/s$. Nonetheless, extensive chain entanglement may suppress the drawability even at temperatures close to crystal melting. Strain rate has an effect similar to temperature,[107,144–148] activation energies of extensional flow and the activation energy of α_c relaxation are of a similar magnitude.

According to Hu and Schmidt - Rohr[144] drawing of polymers with nonductile or low ductile crystals is possible through deformation of amorphous areas, breakdown of crystalline lamellae, partial unwinding of some chains from the mosaic block surfaces, and sliding of the fibrils, that is, by the mechanisms considered for the classical fiber formation processes. Depending on the polymer and a particular morphology, the maximum of the achievable drawing without chain translational motion may be taken as no more than seven times.[144]

The extensive drawing is essential to the processes like solid state extrusion, gel - spun fibers or fibers formed from solution.

IV.6.b Results of Cold Drawing

As a result of cold drawing, the fiber density increases, and in connection with the changes of the entropy, the glass transition temperature also changes.[117] For poly(ethylene terephthalate), glass transition decreases with draw ratio to reach a minimum at $\lambda = 1.5$, later it increases to reach a maximum at $\lambda = 2$ to $2,5$, then further decreases monotonically. The density decreases with the draw ratio to a minimum at $\lambda = 1,5$, where the glass transition has a maximum, but later the density increases monotonically with increasing draw ratio. At very high draw ratios, the density may start to decrease again; if so, this is due to a micro void formation.

As the density increases with draw ratio, so increases the contents of the *trans* configuration of the polymer chains. The last fact indicates that initially the structure is less oriented than in the undrawn material, while at $\lambda > 2$ the amorphous molecules become more and more oriented along the fiber axis and also become more densely packed. These results appear to be in good accord with the X- ray investigations.

Glass transition is believed to be a phenomenon related to the relaxation,

a freezing/unfreezing of micro-Brownian motions, that is being explained either through the free volume theory or through changes in the configurational entropy. Recently the latter explanation seems to be gaining more acceptance.

G. Adam and J. H. Gibbs[118] give the following relationship between relaxation time, τ, and configurational entropy, S_c:

$$\tau = \frac{A}{T \cdot S_c} \tag{IV.79}$$

Configurational entropy is considered to consist of two parts[119]

$$S_c = S_{c1} + S_{c2} \tag{IV.80}$$

where S_{c1} is the entropy associated with the configuration of the molecular chain and S_{c2} is the entropy connected with the intermolecular interaction. Thus, S_{c1} is this portion of configurational entropy, which is sensitive to orientation.

A very significant effect of a cold drawing is the generation of heat. The amount of heat developed due to the mechanical work of drawing may be calculated from[120]

$$W_D = F_D v t_n \tag{IV.81}$$

Here W_D - mechanical work of drawing, F_D - drawing force, v - velocity of drawing, and t_n is the time the material spends in the neck.

Using the AGA Thermovision instrument, J. W. Maher *et al.*[120] have investigated the temperature distribution in a necking zone (figure IV.35). The filament temperature starts increasing at the same point where the filament starts necking, but the *hot spot*, the area where apparently the maximum of heat is developed, is close to the beginning of the necking. It is removed from the beginning of the onset of necking by about one half of the radius of undrawn fiber. The temperature decreases from this spot much faster toward the fiber surface and much slower along the fiber axis.

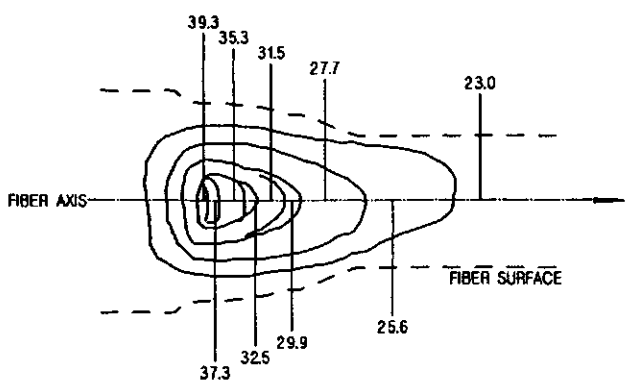

Figure IV.35: *Schematic representation of the temperature distribution in necking. Temperature given in* deg C. *Polymer: polycarbonate. After J. W. Maher et al.*[120]

As there is no reservation to the interesting experimental results, it is difficult to reconcile them with the X-ray investigations of the changes in the crystalline structure mentioned above. There is no doubt that a very large role is being played by the heat losses. Although the authors devote much space to the estimation of such losses, the considerations appear to be grossly incomplete, especially, as no heat conduction within the filament was considered. One may suspect that the heat develops uniformly along the fiber radius, or perhaps even more toward the surface (in agreement with the X-ray results). The net result in the form of a *hot spot* in the center of the fiber seems to be the effect of the heat losses to the filament surface. As usual, heat transfer along the fiber axis is negligible; the extension of the temperature map downstream is a probable result of the mass movement and of the radial heat transfer.

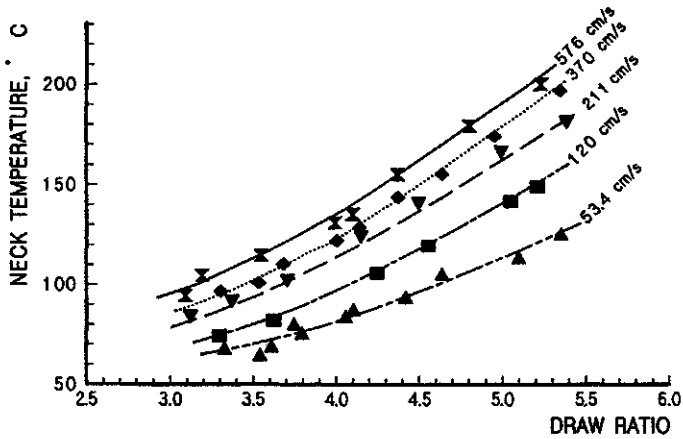

Figure IV.36: *Maximum temperature of necking zone during drawing of nylon 66 to various draw ratios. Drawing velocity in* $cm \cdot s^{-1}$ *given as parameter. Data quoted after Badami et al.*[127]

Exactly how large a role heat transfer plays in necking may be seen in an older work on a determination of the "wholesale" neck temperature in nylon 66.[127] Figure IV.36 presents neck temperature as it depends on the draw ratio and the drawing velocity which is given as a parameter. The figure speaks very loudly about the paramount role of heat exchange in the process. The rate of drawing — *ergo* the heat development, and of the drawing velocity – *ergo* time for the heat transport. Naturally, a balance of these two decides about the final effect.

Some portion of the drawing energy is spent on the bond rupturing. A study of bond rupture in polyethylene[121] shows that the total number of bonds broken in the polymer ranges from 5×10^{17} to $4 \times 10^{18} cm^{-3}$ in drawing at ambient temperature. Though, the values represent only 10^{-3} to 10^{-2} per cent of the total number of backbone bonds. The number is not large, but considering the associated decrease of molecular mass, it is not necessarily negligible. What is more important, in place of the broken bonds, various characteristic groups are formed, mostly carbonyl and vinyl, and it certainly does have an effect on the

fiber properties. It is necessary to take into account that the bond rupture process occurs mainly in the amorphous areas, that is, the tie and link molecules are broken — this weakens the fiber. Here the proportion of breaks to the total number of tie and link molecules is much larger.

The real purpose of this additional operation in fiber formation, of cold drawing, is improvement of physical properties of fibers. As a result of cold drawing, the tensile properties of fibers increase, and this at the expense of transverse properties; e.g., as the tensile strength goes up the abrasion resistance of fiber goes down. On the other hand, an undrawn fiber is mechanically fragile, its dimensions are unstable, it may be easily deformed. And this, from the utility stand point, is highly undesirable. The problem of effects of cold drawing on fiber properties will be discussed in more detail in chapter on fiber properties.

IV.6.c Orientation

The term *orientation* has already been mentioned above several times. Under this term we understand the description of the position of polymer crystals in relation to the fiber longitudinal axis. This is, however only a part of the notion, the *crystalline orientation.* The second part is *amorphous orientation.*

The notion of *amorphous orientation* is somewhat more difficult to define, one may even call it little nebulous. As polymer crystallizes in lammelar fashion, each lamella contains two fold surfaces. The fold surfaces consist of noncrystalline polymer chains looping back and forth, from a crystalline segment and back to a crystalline segment. If the folds were perfectly regular, they would form semicircles and the average orientation between the two fold surfaces would be perfectly circular, or random, without a preferred directionality.

In reality we have also tie molecules spanning from one lamella to another, as well as stretches of polymer chains which, for one reason or another, are not involved in a crystalline lattice. Thus, when we speak of the amorphous orientation, we refer to the irregularities of the fold sites and of the other chain segments, or of whole chains, which are not involved in the crystalline lattice. This type of orientation cannot be measured directly and unambiguously with the analytical techniques available thus far. Only indirect methods are available.

The crystalline orientation is relatively easy to define. It is the degree of alignment of the c - crystalline axis with the fiber axis. Why the c - axis? Because the polymer chains are always aligned parallel, as accurately as the bond angles permit, to the c - crystalline axis. In some cases, the molecules assume a regularly coiled conformation, then the axis of the coil is aligned parallel to the c - axis.

Direction of the crystalline axes may be determined from X-ray diffractograms, and is usually described by $\cos^2 \sigma$. Since we normally deal with a multiplicity of crystals, we must speak of an average orientation $\langle \cos^2 \sigma \rangle$. Here σ is the angle between the c-axis and the fiber axis z. This parameter is evaluated in terms of the orientation of the crystalline lattice plane normals, expressed also in terms of the cosine square. As the angles are used here the angles between the fiber axis

and the normal to a set of *hkl* crystallographic planes (see figure IV.37). The direction of the normal, P, is specified by the angles ϕ and ψ.

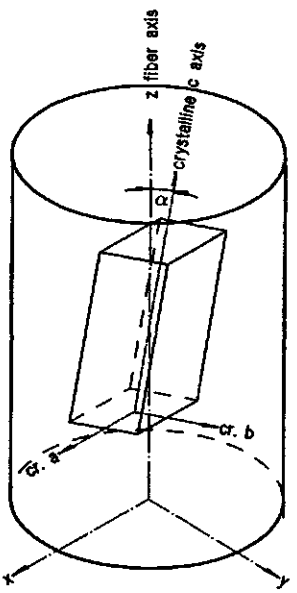

Figure IV.37: *Schematic representation of a crystalline c-axis orientation in relation to the fiber axis z as specified by the angle σ.*

Orientation may be determined from X-ray diffractograms by use of the following set of relations:[122,123]

$$\langle \cos^2 \phi \rangle = \frac{\int_0^{\pi/2} \int_0^{\pi/2} I(\phi,\psi) \cos^2 \phi \sin \phi d\psi d\phi}{\int_0^{\pi/2} \int_0^{\pi/2} I(\phi,\psi) \sin \phi d\psi d\phi} = \frac{\int_0^{\pi/2} I(\phi) \cos^2 \phi \sin \phi d\phi}{\int_0^{\pi/2} I(\phi) \sin \phi d\phi} \tag{IV.82}$$

$$I(\phi) = \int_0^{\pi/2} I(\phi, psi) d\psi \tag{IV.83}$$

$$\langle \cos^2 \sigma \rangle = 1 - \frac{(1 - 2\sin^2 \rho_2)\langle \cos^2 \phi_1 \rangle - (1 - \sin^2 \rho_1)\langle \cos^2 \phi_2 \rangle}{\sin^2 \rho_1 - \sin^2 \rho_2} \tag{IV.84}$$

Here the subscripts 1 and 2 refer to the two considered planes, and ρ is the angle between a plane normal and b-axis. The values of ρ are normally determined from the crystallographic analysis, and they are usually tabulated in literature on crystallographic data.

The determination of orientation by the $\langle \cos^2 \phi \rangle$ is limited, as for a perfectly parallel alignment it is unity and for c-axis normal (90 deg) to the fiber axis it

is zero. To move the description of the orientation closer to the physical reality, Hermans and Platzek[124] have developed the so called *orientation distribution function*, f:

$$f = 1 - \frac{3\sin^2\phi}{2} \equiv \frac{3\langle\cos^2\phi\rangle - 1}{2} \tag{IV.85}$$

According to this designation, a perfect alignment of c-axis with the fiber axis gives $f = 1$, an orientation of c-axis normal (90 deg) to the fiber axis gives $f = -0.5$, while a completely random distribution of the angles results if $f = 0$.

The orientation angle, as well as the distribution function, may be determined in relation to all three Cartesian axes. In such case $f_x + f_y + f_z = 0$.

Use of the orientation distribution function is particularly convenient for fibers with a low or moderate degree of orientation.

Besides wide angle X-ray diffraction and low angle X-ray scattering, there are several other methods of determining orientation in polymeric materials. Perhaps the simplest in execution and the most commonly used is determination of the optical birefringence. The method is based on the measurement of the refractive index difference in both the direction of fiber axis and perpendicular to it. Nevertheless, the birefringence is not a singular property determined by one factor only. In general, one may describe it as follows:

$$\Delta n = \sum \phi_i \Delta n_i^{phase} + \Delta n_f + \Delta n_\varepsilon \tag{IV.86}$$

where ϕ means volume fraction of different phase material. Birefringence may vary according to phase: crystalline, paracrystalline, amorphous, variable density, leave alone additives. Further, Δn_f represents birefringence of form: it is variations arising on the boundaries of phases or when the electric field, or dipole, is distorted by whatever cause. Δn_ε represents changes of the birefringence due to strain, a factor influencing the birefringence very strongly.

The orientation distribution function, f, (equation IV.85) is equal to the ratio of a specimen birefringe over the maximum obtainable birefringence for a given polymer. The last number represents a calculated quantity, which may be found tabulated in literature. Occasionally it happens, however, that highly drawn fibers show birefringence higher than the theoretical maximum. If this happens, it indicates invariably the presence of frozen internal stresses, and if so, the measured values must be deemed as quite useless.

Separation of the different reasons for change in birefringence is very difficult, often outright impossible. This, in combination with the relative simplicity of the determinations cause this method of orientation determination to be highly overused, which leads to many misinterpretations. A method of "micro determination" of birefringence, that is, variation of birefringence along fiber radius may offer some help in this respect. This method was proposed by Beier and Schollmeyer.[126]

Another way to determine orientation is by way of measurement of infrared (IR) dichroism. Certain bands in the IR spectrum, which are not affected by molecule conformation, may absorb polarized IR radiation selectively in a certain

plane. If such bands are present in a polymer, one may measure the ratio of intensity of polarized infrared light transmitted to the incident beam, when the measurements of the polarization direction are made in both perpendicular and parallel directions to the fiber axis. A dichroic ratio may be calculated as

$$R = \frac{\ln(I_0/I_{\parallel})}{\ln(I_0/I_{\perp})} \tag{IV.87}$$

where I_0 is the intensity of the incident beam, and $I_{\parallel}$ and $I_{\perp}$ are the intensities of the transmitted light parallel and perpendicular to the fiber axis. From the dichroic ratio, R, one may calculate the orientation function distribution:

$$f = \frac{(R-1)(R^{\infty}+2)}{(R^{\infty}-1)(R+2)} \tag{IV.88}$$

R^{∞}, the dichroic ratio for the perfect orientation may be calculated when the dipole connected to a specific group in oriented polymer oscillates at a right angle to the polymer chain axis.

Still another way of determining orientation is based on the fact that sound velocity in a material depends on the distances between atoms. Usually the distances in the main chain backbone differ from the distances between atoms of the neighbor polymer chains. For determination of orientation, it is necessary to know the sound velocity parallel and perpendicular to the fiber axis for the case of perfectly oriented polymer. Velocity parallel for polymers usually ranges between some 7 and $10 km/s$. The parallel velocity is usually either calculated theoretically or just estimated. The general relationship for the velocities is:[125]

$$\frac{1}{c^4} = \frac{1-\langle\cos^2\phi\rangle}{c_{\perp}^2} + \frac{\langle\cos^2\phi\rangle}{c_{\parallel}^2} \tag{IV.89}$$

In a completely random sample, when $f = 0$, according to equation IV.85 $\langle\cos^2\phi\rangle = 1/3$. Substituting this value into equation IV.89 gives

$$c_{\perp}^2 = \frac{2c_{\circ}^2 c_{\parallel}^2}{3c_{\parallel}^2 - c_{\circ}^2} \tag{IV.90}$$

In the above equations, c is velocity of sound, subscripts $\parallel$, $\perp$, and $\circ$ mean parallel, perpendicular, and randomly oriented, respectively. Since in all cases known so far $3c_{\parallel}^2 \gg c_{\circ}^2$ applies, then the value of perpendicular velocity calculated from an assumed value of parallel velocity and equation IV.90 is relatively little sensitive to the assumed value of parallel velocity, if it is the case. In view of this, equation IV.90 simplifies to:

$$c_{\perp}^2 = \frac{2c_{\circ}^2}{3} \tag{IV.91}$$

and equation IV.89 simplifies to

$$\frac{1}{c^2} = \frac{1-\langle\cos^2\sigma\rangle}{c_{\parallel}^2} \tag{IV.92}$$

In the end, the orientation distribution factor is:

$$f = 1 - \frac{c_\circ^2}{c^2} \tag{IV.93}$$

All the methods described, besides X-ray, give orientation of both crystalline and amorphous material. All of the methods are more or less sensitive to any residual stresses. To separate the crystalline and amorphous components, one must have X-ray determination plus analysis by any of the other techniques.

IV.7 Annealing

That crystals may be annealed, as well as what kind of changes the annealing process triggers, was mentioned in the section on polymer crystals. In fiber formation, advantage is taken of the annealing. Mostly it is done immediately after cold drawing, or sometimes it is considered even as an additional step of the cold drawing operation. The drawn fibers are crystalline structures which are oriented, and the orientation adds one more dimension to the annealing process.

Oriented structures may be annealed in two different ways: with or without a dimensional restrain. If the annealing process is conducted without the dimensional restrain, the fiber will shrink, and the shrinkage will increase with the increasing draw ratios and annealing temperature, but will decrease with increasing drawing temperature. If the shrinkage is prevented by mechanical restrain, there are still changes in the fiber structure that take place, though the changes will be somewhat different, and their influence on the material properties will also be different.

A fiber annealed with restrain will, obviously, not shrink, but crystalline orientation will decrease, and amorphous orientation usually decreases even more. Without restrain, all other conditions being equal, the *disorientations* are much larger, particularly the crystalline one.

The fiber's succeptibility, if one may call it so, to annealing depends strongly on the relationship of the temperature of original crystallization and temperature of cold drawing on one side, and on the temperature and time of annealing on the other side.

In some sense, annealing may be treated as a kind of "preshrinking", a way to prevent fiber shrinkage in its final use. Such treatment, however, is accompanied by change of another fiber properties, like tenacity, moduli, especially the initial modulus, orientation, density, dying characteristic, *etc.* A slight extension during annealing, sometimes treated as an additional drawing step, often prevents an excessive decrease of properties with a simultaneous gain in thermal stability of the fiber.

Every annealing process, irrespectively of restrain or lack of it, always leads to an increase in crystalline melting point of the polymer.

It may seem convenient to anneal fibers in a continuous operation with drawing, but this creates problems of its own. The annealing process is slow and therefore

it may be difficult to accommodate it in one line with the contemporary fast processes. A way to overcome such difficulties to some extent may be to apply a so called *heat shock*. This means application of high temperature, often above crystalline melting point, but over a short time. One may consider it as intensification of heat transfer to the fiber. In the same vein, a steam atmosphere may be applied in the annealing process.[128] Even liquids, like silicone oils and similar, have been applied for the same purpose.[129]

IV.8 References

1. Z. K. Walczak, *paper presented at the 70-th Annual A.I.Ch.E. Meeting*, Atlantic City, **Sept. 1, 1971**; *J. Appl. Polymer Sci.*, **17 (1973)**, 153. 1
2. R. Farber and J. Dealy, *Polymer Eng. Sci.*, **14 (1974)**, 435.
3. W. W. Grassley, *Adv. Polymer Sci.*, **16 (1974)**, 1.
4. S. F. Edwards, *J. Phys. A, Gen. Phys.*, **1 (1968)**, 15; P. G. de Gennes, *J. Chem. Phys.*, **55 (1971)**, 572; M. Doi, S. F. Edwards: *The Theory of Polymer Dynamics*, Oxford Univ. Press, Oxford, 1986.
5. H.-G. Elias, *Macromol. Chem., Phys.*, **195 (1994)**, 3117.
6. R. P. Wool, *Macromolecules*, **26 (1993)**, 1564.
7. S. Wu, *J. Polymer Sci.: B. Polymer Phys.*, **27 (1989)**, 723.
8. C. D. Han and K. U. Kim, *Polymer Eng. Sci.*, **11(1971)**, 395.
9. C. D. Han, *J. Appl. Polymer Sci.*, **17 (1973)**, 1403. 9
10. E. B. Bagley, *J. Appl. Phys.*, **28 (1957)**, 624.
11. C. D. Han and R. R. Lamonte, *Polymer Eng. Sci.*, **11 (1971)**, 385.
12. Z. K. Walczak: *Formation of Synthetic Fibers*, Gordon and Breach, London - New York, 1977, p. 55.
13. Z. K. Walczak, *J. Appl. Polymer Sci.*, **17 (1973)**, 169, 177.
14. P. J. Hendra, M. A. Taylor, H. A. Willis, *J. Polymer Sci.: Pt. C: Polymer Letters*, **24 (1986)**, 83.
15. P. Massa, A. Ten Bosch, P. Sixou, *J. Polymer Sci., Polymer Letters*, **21 (1983)**, 757.
16. A. Ziabicki: *Fizyka procesw formowania włókna*, Wydawnictwa Naukowo-Techniczne, Warszawa, 1970 (in Polish). (Physics of fiber formation processes)
17. A. Ziabicki: *Fundamentals of Fibre Formation*, John Wiley & Sons, New York - London - Sydney, 1976.
18. H. Nitschmann and J. Schrade, *Helv. Chim. Acta*, **31 (1948)**, 297.
19. F. T. Trouton, *Proc. Royal Soc. (London)*, **A77 (1906)**, 426.
20. N. Hirai, *J. Chem. Soc. Japan*, **75 (1954)**, 1021.
21. R. Gatoh, A. Aida, S. Hayashi, and N. Hirai, *Rheol. Acta*, **1 (1958)**, 213.
22. G. Fano, *Arch. fisiol.*, **5 (1908)**, 365.
23. M. Zidan, *Rheol. Acta*, **8 (1969)**, 89.
24. C. J. S. Petrie: *Elongational flows*, Pitman Publ., London, 1979.

25. F. N. Cogswell, *J. Non - Newtonian Fluid Mechanics*, **4 (1978)**, 23.

26. B. H. Bersted, *Polymer Eng. Sci.*, **33 (1993)**, 1079.

27. S. Goldstein: *Modern Developments in Fluid Mechanics*, Oxford University Press, London, 1952.

28. S. Zahorski in *Theoretical Rheology*, in J. F. Hutton, J. R. A. Pearson and K. Walters (Eds.), Appl. Science Publ., London, 1975, p. 40.

29. M. Reiner and A. Freudenthal, *Proc. of Fifth International Congress on Applied Mechanics*, 1938.

30. A. Kaye, D. G. Vale, *Rheol. Acta*, **8 (1969)**, 1.

31. N. V. Tschoegl, *Phenomenological Theory of Linear Viscoelastic Behavior*,Springer Verlag, Berlin - Heidelberg - New York, 1989.

32. G. V. Vinogradow, A. Ya. Mal'kin: *Reol'ogiya polimerov* (Rheology of Polymers), Izdatelstvo Chimiya, Moskva, 1977; *Rheology of Polymers*, Springer Verlag, Berlin - Heidelbeg - New York, 1980.

33. G. V. Vinogradov, V. D. Fikhman, B. V. Radushkevich, and A. Ya. Mal'kin, *J. Polymer Sci., Pt. A - 2*, **8 (1970)**, 657.

34. V. A. Kargin and T. I. Sogol'ova, *Zh. Phiz, Khim.*, **23 (1949)**, 540.

35. T. Alfrey: *Mechanical Behavior of High Polymers*, Interscience Publ., New York, 1948.

36. G. V. Vinogradov, *Rheol. Acta*,**12 (1975)**, 557; **14 (1975)**, 942.

37. T. L. Smith, *J. Polymer Sci*, **32 (1958)**, 99.

38. E. Orowan, *Rep. Prog. Phys.*, **12 (1949)**, 186.

39. H. Chung and A. S. Lodge, *Rheol. Acta*, **10 (1971)**, 448; **11 (1972)**, 127.

40. Y. Ide and J. L. White, *J. Appl, Polymer Sci.*, **20 (1976)**, 2511.

41. Y. Ide and J. L. White, *J. Non-Newtonian Fluid Mech.*, **2 (1977)**, 281.

42. D. Acierno, F. P. La Mantia, G. Iorio, G. Marucci, *J. Non- Newtonian Fluid Mech.*, **4 (1978)**, 99.

43. G. Marucci, G. Titomanlio, and G. C. Sarti, *Rheol. Acta*, **12 (1973**, 269.

44. D. Acierno, F. P. La Mantia, G. Marucci, and G. Titomanlio, *J. Non-Newtonian Fluid Mech.*, **1 (1976)**, 1.

45. D. Acierno, F. P. La Mantia, G. Marucci, and G. Titomanlio, *J. Non-Newtonian Fluid Mech.*, **1 (1976)**, 147.

46. D. Acierno, F. P. La Mantia, G. Marucci, and G. Titomanlio, *J. Non-Newtonian Fluid Mech.*, **2 (1977)**, 271.

47. J. Ferguson and N. E. Hudson, *Eur. Polymer J.*, **29 (1993)**, 141.

48. N. Phan - Thien and R. I. Tanner, *J. Non-Newtonian Fluid Mech.*, **2 (1977)**, 353.

49. N. Phan - Thien, *J. Rheology*, **22 (1978)**, 259.

50. J. A. Spearot, *PhD Dissertation*, University of Delaware, Newark, Delaware, **1972.**

51. G. R. Zeichner, *M. Ch. E. thesis*, University of Dalaware, Newark, Delaware, **1973.**

52. A. J. Stavermann and F. Schwartzl *Non Linear Deformation Behaviour of High Polymers*, in H. A. Stuart (Ed.):*Die Physik der Hochpolymeren*, Vol IV, chapter 2., Springer Verlag, Berlin - Heidelberg, New York, 1954.

53. K. Weissenberg, *cited in ref. 54, p.128.*

54. J. D. Ferry: *Viscoelestic Properties of Polymers*, John Wiley & Sons Publ., New York, 1980.

55. A. J. Stavermann and F. Schwartzl *Linear Behaviour of High Polymers*, in H. A. Stuart (Ed.):*Die Physik der Hochpolymeren*, Vol IV, chapter 1., pp. 59 ff., Springer Verlag, Berlin - Heidelberg, New York, 1954.

56. J. R. Clermont, J. M. Pierrad, and O. Scrivener, *J. Non- Newtonian Fluid Mech.*, **1 (1976)**, 175.

57. D. D. Goulden and W. C. MacSporran, *J. Non-Newtonian Fluid Mech.*, **1 (1976)**, 183.

58. R. Keunings, M. J. Crochet, and M. M. Denn, *Ind. Eng. Chem., Fundam.*, **22 (1983)**, 347.

59. M. A. Matovich and J. R. A. Pearson, *Ind. Eng. Chem., Fundam.*, **8 (1969)**, 512.

60. J. R. A. Pearson, and M. A. Matovich, *Ind. Eng. Chem., Fundam.*, **8 (1969)**, 605.

61. Y. T. Shah and J. R. A. Pearson, *Ind. Eng. Chem., Fundam.*, **11 (1972)**, 145.

62. J. R. A. Pearson and Y. T. Shah, *Ind. Eng. Chem., Fundam.*, **13 (1974)**, 134.

63. Ref. 25, pp. 199 ff.

64. G. V. Vinogradov, *Rheol. Acta*, **12 (1973)**, 273.

65. Jinan Cao, *J. Appl. Polymer Sci.*, **42 (1991)**, 143; **49 (1993)**, 1759.

66. K. Katayama, T. Amano, and K. Nakamura, *Appl. Polymer Symposia*, **20 (1973)**, 237.

67. A. Nowakowski, *Technology of Plastics and Synthetic Fibers*, Lectures at The Polytechnic of Łódź, 1953.

68. A. K. Van der Vegt and P. P. A. Smit, *Soc. Chem. Ind. (London), Monograph No. 26*, 1967, p. 313.

69. *ref. 12*, p. 100.

70. Z. K. Walczak, *unpublished results*, **(1976)**; *Thermal Bonding of Fibers*, Published by Kimberly-Clark Corp., 1992, p. 135.

71. G. A. Korn and T. M. Korn: *Mathematical Handbook for Scientists and Engineers*, McGraw Hill Publ., New York, 1961, Chapter 4.11-3, 8.7-1, 18.10-10, 20.3-6.

72. J. W. Cahn, *Acta Met.*, **10 (1962)**, 907.

73. J. E. Hilliard, in *Nucleation Phenomena*, ACS Publications, Washington, 1966, p. 77 ff.

74. K. Nakamura, T. Watanabe, K. Katayama, and T. Amano, *J. Appl. Polymer Sci.*, **16 (1972)**, 1077.

75. K. Nakamura, K. Katayama, and T, Amano, *J. Appl. Polymer Sci.*, **17 (1973)**, 1031.

76. A. Ziabicki, *Colloid Polym. Sci.*, **252 (1974)**, 207.

77. G. Eder and H. Janeschitz-Kriegl, *Colloid Polym. Sci.*, **266 (1988)**, 1087.

78. V. Brucato, S. Piccarolo, G. Titomanlio, *Makromol. Chem., Makromol. Symp.*, **68 (1993)**, 245.

79. A. Mehta, B. Wunderlich, *ACS Polymer Preprints*, **35 (1975)**, 393.

80. W. H. Carothers and J. W. Hill, *J. Am. Chem. Soc.*, **54 (1932)**, 1579.

81. F. H. Müller, *Kolloid Z.*, **114 (1949)**, 59; cit in *Die Physik der Hochpolymeren*, H. A. Stuart (Ed.), Springer Verlag, Berlin - Heidelberg - Wien, 1956, Vol. IV, p. 161.

82. E. Orowan, *Rep. Prog. Phys.*, **12 (1948)**, 185.

83. P. I. Vincent, *Polymer*, **1 (1960)**, 7.

84. A. Ziabicki, K. Kędzierska, *Kollid Z.*, **171 (1960)**, 51.

85. S. Kase, T. Matsuo, *J. Polym. Sci.*, **A3 (1965)**, 2541. 85

86. S. Kase, T. Matsuo, *J. Appl. Polymer Sci.*, **11 (1967)**, 251.

87. Y. Wada, A. Nakayama, *J. Appl. Polymer Sci.*, **15 (1971)**, 183.

88. J. L. Ericksen, *J. Elasticity*, **5 (1975)**, 191.

89. M. M. Denn, C. J. S. Petrie, P. Avenas, *AIChE J.*, **21 (1975)**, 791.

90. A. Considere, Ann. des pots des chausees, **ser. 6. No. 9**, 574.

91. B. Bernastein and L. J. Zapas, *J. Rheol.*, **25 (1981)**, 83.

92. B. Bernastein, E. A. Kearsley, and L. J. Zapas, *Trans. Soc. Rheol.*, **7 (1963)**, 391

93. B. D. Coleman and D. C. Newman, *J. Appl. Polymer Sci.*, **45 (1992)**, 997.

94. B. D. Coleman and D. C. Newman, *J. Polymer Sci., Pt. B, Polymer Physics*, **30 (1992)**, 25.

95. S. Kase, M. Chang, *Rheol. Acta*, **29 (1990)**, 46,

96. A. I. Leonov, *J. Rheol.*, **34 (1990)**, 155.

97. E. Oleinik, *Prog. Colloid Polym. Sci.*, **80 (1989)**, 140.

98. S. N. Rudnev, O. B. Salamantina, V. V. Vaenniy, and E. F. Oleinik, *Colloid Polym. Sci.*, **269 (1991)**, 460.

99. R. N. Howard, *Polymer*, **35 (1994)**, 3858.

100. R. N. Howard, *J. Polymer Sci, Pt B, Polymer Physics*, **3 (1995)**, 1481.

101. *cit in* A. Nadai, *The Theory of the Fracture and Flow of Solids*, McGraw - Hill, New York, 1950, p. 71.

102. P. I. Vincent, *Polymer*, **1 (1960)**, 7.

103. J. M. Andrews and I. M. Ward, *J. Mater. Sci.*, **5 (1970)**, 411.

104. J. S. Foot and I. M. Ward, *J. Mater. Sci.*, **10 (1975)**, 953.

105. F. Geleji, L. Koczy, I. Fulop, and G. Bodor, *J. Polymer Sci, Polymer Symp.*, **58 (1977)**, 253.

106. J. C. Engelaere, J. P. Cavrot, and F. Rietch, *Polymer*, **23 (1982)**, 766.

107. D. M. Sadler and P. J. Barham, *Polymer*, **31 (1990)**, 36.

108. P. I. Vincent, *Proc. Conf. Physical Basis of Yield and Fracture*, Oxford, 1966; Inst. of Physics and Phys. Soc., London, p. 155.

109. G. R. Williamson, B. Wright, and R. N. Haward, *J. Appl. Chem.*, **14 (1964)**, 131.

110. A. Marquez - Lucero, C. G'Sell, and K. W. Neale, *Polymer*, **30 (1989)**, 636.

111. R. H. Butler, D. C. Prevorsek, and Y. D. Kwon, *Polymer Eng. Sci.*, **2 (1982)**, 329.

112. N. Kasai and M. Kakudo, *J. Polymer Sci., Pt. A*, **2 (1964)**, 1955.

113. S. L. Aggarval, G. P. Tilley, and O. J. Sweeting, *J. Polymer Sci.*, **51 (1961)**, 551; *J. Appl. Polymer Sci.*, 1 **(1959)**, 91.

114. V. S. Kuksyenko, S. Nizamidinov, and A. I. Slutsker, *Vysokomol. Soyed.*, **9 (1967)**, 91.
115. L. R. G. Treloar, *The Physics of Rubber Elasticity*, Oxford Univ. Press, London, 1975.
116. E. R. Story, J. N. Hay, *Polymer Communications*, **29 (1988)**, 9.
117. E. Ito and T. Hatakeyama, *J. Polymer Sci., Polymer Phys. Ed.*, **12 (1974)**, 1477.
118. G. Adam and J. H. Gibbs, *J. Chem. Phys.*, **43 (1965)**, 139.
119. T. Nose, *Polymer J.*, **2 (1971)**, 124; 427; 437.
120. J. W. Maher, R. N. Haward, and J. N. Hay, *J. Polymer Sci., Polymer Phys. Ed.*, **18 (1980)**, 2169.
121. C. L. Hammond, P. J. Hendra, B. G. Lator, W. F. Maddams, and H. A. Willis, *Polymer*, **29 (1988)**, 49.
122. O. Kratky, *Z. physik. Chem.*, **B50 (1941)**, 255.
123. Z. W. Wilchinsky, *J. Appl. Phys.*, **30 (1959)**, 792; **31 (1960)**, 1969; *Polymer*, **5 (1964)**, 271.
124. P. H. Hermans and P. Platzek, *Kolloid Z.*, **88 (1939)**, 68.
125. H.-G. Elias, *Macromolecules*, Plenum Press Publ., New York - London, 1984, p. 192 ff.
126. M. Beier and E. Schollmeyer, *Angew. Makromol. Chem.*, **128 (1984)**, 15.
127. D. V. Badami, F. P. Chappel, M. F. Culpin, D. Madoc Jones, and T. C. Tranter, *Rheol. Acta*, **1 (1961)**, 639.
128. P. H. Geil, *Polymer Single Crystals*, Interscience publ., New York, 1963, p. 424.
129. D. R. Buchanan and J. D. Dumbleton, *J. Polymer Sci., Pt. A-2*, **6 (1969)**, 113.
130. I. G. Voigt-Martin, *Adv. Polymer Sci.*, **67 (1985)**, 196.
131. M. Okamoto, H.Kubo, and T. Kataoka, *Polymer*, **39 (1998)**, 3135.
132. C. P. Buckley and D. P. Jones, *Polymer*, **36 (1998)**, 3301.
133. A. M. Adams, C. P. Buckley, and D. P. Jones, *Polymer*, **39 (1998)**, 5761.
134. J. W. H. Kolnaar, A. Keller, S. Seifert, C. Zschunke, and H. G. Zachmann, *Polymer*, **36 (1995)**, 3969.
135. J. Furukawa, *J. Appl. Polymer Sci.*, **57 (1995)**, 1085; 1095.
136. A. V. Pendse and J. R. Collier, *J. Appl. Polymer Sci.*, **59 (1996)**, 1305.
137. J. R. Collier, O. Romanoschi, and S, Petrovan, *J. Appl. Polymer Sci.*, **69 (1998)**, 2357.
138. W. A. Kernick III and N. J. Wagner, *Macromolecules*, **32 (1999)**, 1159.
139. M. M. Denn: *Process Modeling*, Longman – Wiley, London – New York, 1986.
140. B. M. Devereux, M. M. Denn, *Ind. Eng. Chem. Res.*, **33 (1994)**), 2384.
141. J.–F. Agassant, P. Avenas, J.–Ph. Sergent, P. J. Carreau: *Polymer Processing: Principles and Modelling*, Hanser Verlag, München, 1991.
142. G. Vassilatos, E. R. Schmelzer, and M. M. Denn, *Int. Polymer Process.*, **7 (1992)**, 144.
143. J. Fisher and D. Turnbull, *J. Chem. Phys.*, **17 (1949)**, 71.
144. W. G. Hu and K. Schmidt - Rohr, *Acta Polym.*, **50 (1999)**, 271.
145. I. F. Govaert and P. J. Lemstra, *Coll. Polymer Sci.*, **270 (1992)**, 455.

146. R. H. Boyd, *Polymer*, **26 (1988)**, 323.

147. S. Bensason, J. Minick, A. Moet, S. Chum, A. Hiltner, and E. Baer, *J. Polymer Sci., Part B, Polymer Phys.*, **34 (1996)**, 1301.

148. W. T. Mead and R. S. Porter, *J. Polymer Sci., Polymer Symp.*, **63 (1978)**, 289.

149. A. Ya. Malkin and C. J. S Petrie, *J. Rheol.*, **41 (1997)**, 1.

150. V. Tirtaamadja abd T. Sridhar, *J. Rheol.*, **39 (1995)**, 1133.

151. P. Flory, *Principles of Polymer Chemistry*, Cornell University Press, Ithaca, NY, 1953.

152. *ref. 54*, p. 262.

153. A. Mahendrasingam, C. Martin, F. Fuller, D. J. Blundell, R. J. Oldman, J. L. Harvie, D. H. MacKerron, C. Riekel, P. Engström, *Polymer*, **40 (1999)**, 5553,

154. T. Asano, F. J. Baltá Calleja, A. Flores, M. Tanigaki, M. F. Mina, C. Sawatari, H. Itagaki, H. Takahashi, I, Hatta, *Polymer*,, **40 (1999)**, 6475.

155. Y. Termonia, *J. Polymer Sci., Pt. B, Polymer Phys.*, **38 (2000)**, 2422.

156. N. V. Tschoegl, *Phenomenological Theory of Linear Viscoelastic Behavior*,Springer Verlag, Berlin - Heidelberg - New York, 1989, Chapter 10.